

# 1 Intensified upwelling: normalized sea surface temperature trends

## 2 expose climate change in coastal areas

3 Miguel Ángel Gutierrez-Guerra<sup>1,2</sup>, María Dolores Pérez-Hernández<sup>1</sup>, Pedro Vélez-Belchí<sup>2</sup>

4 <sup>1</sup> Unidad Océano y Clima, Instituto de Oceanografía y Cambio Global, IOCAG, Universidad de Las Palmas de Gran Canaria,  
5 ULPGC, Unidad Asociada ULPGC-CSIC, Canary Islands, Spain

6 <sup>2</sup> Centro Oceanográfico de Canarias, Instituto Español de Oceanografía, Santa Cruz de Tenerife, Canary Islands, Spain

7 *Corresponding author:* Miguel A. Gutierrez-Guerra, miguel.gutierrez104@alu.ulpgc.es

8

### 9 **Abstract.**

10 The Eastern Boundary Upwelling Systems (EBUS) provide valuable natural resources due to their high  
11 primary production. However, there is significant uncertainty in how climate change may affect the  
12 mechanisms that sustain these ecosystems in the future. Therefore, assessing the effects of climate change  
13 on the EBUS under the current global warming scenario is crucial for efficient ecosystem management.  
14 In 1990, Andrew Bakun suggested an increase in the upwelling intensity due to the rise of the ocean-land  
15 pressure gradient. Since there is a significant link between thermal gradients and offshore Ekman  
16 transport, we use sea level pressure and deseasonalized sea surface temperature (SST) data from remote  
17 sensing to elucidate this hypothesis and validate it using in-situ observations. SST is an indicator of coastal  
18 upwelling, and our long-term analysis of monthly and deseasonalized SST records shows that the seasonal  
19 and synoptic processes have minimal influence on the SST-upwelling intensity relationship. Upwelling  
20 within the same EBUS is not usually evenly distributed along coastlines, leading to upwelling in specific  
21 areas, upwelling centers. We compare the SST trends in the main upwelling centers of the four EBUS  
22 with those in open ocean waters through a new index,  $\alpha_{UI}$ , designed to characterize upwelling changes in  
23 the EBUS. An adimensional number allows us to normalize the trends independently of the upwelling  
24 system and compare all of them. Furthermore, we have complemented the SST index with sea level  
25 pressure gradient data. This new index (supported by SLP gradient trends) indicates intensification in all  
26 the EBUS, revealing a coherent pattern within EBUS in the same ocean (i.e., Canarian and Benguela or  
27 Californian and Humboldt Upwelling Systems).

28 **1. Introduction**

29 The world's major coastal upwelling areas exist along the eastern margins of the Pacific and the Atlantic  
30 Oceans. These extended coastal upwelling systems are known as Eastern Boundary Upwelling Systems  
31 (EBUS) and sustain the most important fisheries in the world (Pauly and Christensen, 1995). The rise of  
32 cool, nutrient-rich waters supports the high primary production needed to maintain these complex  
33 ecosystems (Ekman, 1905). Their economic and ecological relevance explains the association of the  
34 EBUS with the world's major Large Marine Ecosystems (LME) (Fig 1). LME are a globalized approach  
35 to a management framework that defines and ranks marine regions based on their gross primary  
36 production (Sherman and Hempel, 2008), and four of the largest LME are embedded in the EBUS  
37 worldwide (Kämpf and Chapman, 2016).

38 Bakun, (1990) hypothesized that the sea-land temperature gradient will increase under climate change  
39 and therefore, it should increase the upwelling intensity. The hypothesized increase in the temperature  
40 gradient arises from an increased atmospheric pressure gradient between the low-pressure cell that  
41 develops over the heated land mass and the high-pressure cell existing over the colder ocean. Therefore,  
42 as the land warms faster than the ocean, it enhances the low-pressure cells. Thus, the increase in the  
43 pressure gradient drives more intense upwelling favorable winds, intensifying the cold imprint in the Sea  
44 Surface Temperature (SST) near the shore. However, previous studies that have tested Bakun's hypothesis  
45 with in-situ data have found contradictory long-term trends (Barton et al., 2013; Belkin, 2009; McGregor  
46 et al., 2007; Rykaczewski et al., 2015; Sambe et al., 2016).

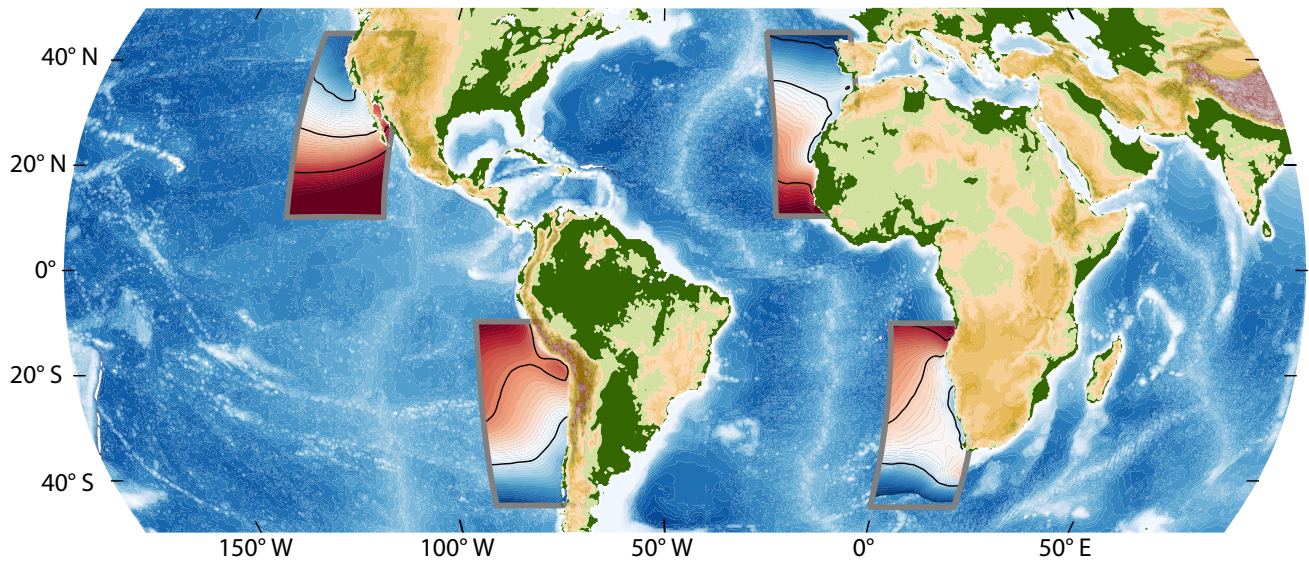


**Fig 1: Location of the EBUS (colored areas) in the world, associated with eastern boundary currents. For each region, the enclosed area includes the mean SST from 1982-2022.**

47 Sydeman et al., (2014) performed a meta-analysis of 18 trends obtained from independent studies of wind  
 48 stress, both from observational and model data. Observational data were more likely to report an increase  
 49 in wind stress in the four EBUS than model data (excluding Benguela, where no observations were  
 50 considered). However, the model data were less consistent between EBUS, showing agreement with  
 51 observations only in the case of the California system (both supporting intensification) and for the Iberian  
 52 system (with a consistent weakening of the wind stress). García-Reyes et al., (2015) also remarked that  
 53 in climate change models, the upwelling-related cooling trends were difficult to reproduce due to the  
 54 small spatial scale of the coastal upwelling process. Such a controversy between the model, and different  
 55 observations reflects the complexity of EBUS dynamics.

56 Upwelling within the same EBUS is not usually evenly distributed along coastlines because of irregular  
 57 coastlines and seafloors, leading to more pronounced upwelling in specific areas known as 'upwelling  
 58 centers' (Kämpf and Chapman, 2016). These centers are characterized by strong frontal areas and  
 59 upwelling jets that create eddies. In these areas, the sea surface temperature drops due to the upwelling of  
 60 cold subsurface water. Therefore, the relationship between sea surface temperature (SST) and the  
 61 upwelling intensity is more robust in these upwelling centers. Even in cases where a generalized increase  
 62 in favorable upwelling winds occurs, the appearance of cold SST cores, associated with increased

63 upwelling intensity, remains predominantly confined to these specific areas. Therefore, to study the long-  
64 term changes in the upwelling, a good approach is to focus on these representative upwelling areas within  
65 the EBUS since they show a higher signal-to-noise ratio between the SST and Ekman transport.  
66 The main motivation of this study is to assess the impacts of climate change on the four EBUS. This is  
67 pursued by using satellite-derived SST trends as a proxy for changes and a new index that normalizes the  
68 upwelling trend of the coastal upwelling with the oceanic background trends. Specifically, we have  
69 chosen points representative of each dynamical regime at each EBUS: offshore oceanic waters (OC1),  
70 non-upwelling (DW1) areas nearshore, and upwelling centers (UP1 and UP2). These points were chosen  
71 based on the consistency of the year-round upwelling centers deduced from the mean SST field and the  
72 relevance of the area as spawning and nursery emplacements for the pelagic fisheries associated with  
73 upwelling centers. Then, we compare the SST trends in the main upwelling centers of the four EBUS  
74 with those in open ocean waters through a new index,  $\alpha_{UI}$ , designed to characterize upwelling changes in  
75 the EBUS, following Bakun's (1990) hypothesis. The manuscript is organized as follows: sections 2 and  
76 3 describe the dataset and the analysis carried out in the study. Section 4 describes the relevant results,  
77 and the results are discussed and contrasted with other studies, and finally, Section 5 summarizes and  
78 presents the conclusions.

## 79 **2. Data**

80 We based our study on the SST blended analyses for sea surface temperature of the National Ocean and  
81 Atmosphere Administration (NOAA) (Reynolds et al., 2007), which combines SST satellite retrievals  
82 with in-situ measures from ships and buoys. This dataset has a spatial resolution of  $0.25^\circ$  and covers  
83 nearly 40 years (from 1982 to 2021). Following Barton et al. (2013), the 40-years used in this study allow  
84 us to estimate significant trends. Their analysis involved a comprehensive examination of both wind stress  
85 and SST. They segmented these datasets into various subsets of different lengths. Within this analysis,  
86 the trends derived from wind datasets are not significantly different from zero for all considered subset  
87 periods.

88 In contrast, SST trends demonstrated statistical significance with a dataset of 40-years length. In addition,  
89 we incorporated reliable in-situ data in the North Pacific and the North Atlantic oceans for validation.

90 These records were obtained from the National Buoy Data Center (NDBC) and the CalCOFI (California  
91 Cooperative Fisheries Investigations) program for the Pacific. For the Atlantic, the data were gathered  
92 from Puertos del Estado and the RaProCan (Radial Profunda de Canarias) observational program of the  
93 Spanish Institute of Oceanography in the Canary Islands (Tel et al., 2016). The in-situ data, limited to the  
94 northern hemisphere, is used to validate the satellite observations. Given the significantly larger amount  
95 of sampling density existing in the Pacific Ocean compared to the Atlantic Ocean, a lower error is  
96 expected in the reanalysis for the Pacific Ocean. We have also used the EN4 (ENhanced ocean data  
97 assimilation and climate Prediction) dataset from the Met Office Hadley Centre (Good et al., 2013), a  
98 collection of global observations from diverse sources interpolated into a monthly product and a spatial  
99 resolution of 1°. Due to the limited sampling in the cruise data, we cannot align it with the monthly  
100 resolution of the EN4 product. To maintain statistical rigor, we choose not to employ the cruise data for  
101 the validation of EN4.

102 Additionally, two sea level pressure (SLP) datasets are used: the NCEP and ERA5 reanalysis data. The  
103 ERA5, from the European Centre for Medium-Range Weather Forecasts, offers a high resolution of ~0.25  
104 degrees and uses advanced data assimilation methods, covering the period from 1950 to present. While  
105 the NCEP/NCAR Reanalysis, from the National Centers for Environmental Prediction and the National  
106 Center for Atmospheric Research, offers a resolution of 2.5 degrees and uses covering the period from  
107 1948 to present.

### 108 **3. Method**

#### 109 **3.1. Selection of Representative Dynamical Regimes in EBUS.**

110 We have selected areas representative of the different dynamical regimes for further analysis, to avoid  
111 mixing observations in dynamically different areas. Areas UP1 and UP2 are round-year upwelling  
112 centers. The DW1 are areas of convergence where the upwelling does not dominate on an annual average,  
113 and these areas are characterized by higher SST averages than those in the upwelling centers. The OC1  
114 is representative of open ocean (>100km offshore) areas with trends driven by Global Warming. Given

115 the distinctive and unique features that characterised each EBUS, as commented in Section 1, we based  
116 the selection of the representative locations on the literature and the SST mean field (Fig. 2):

### 117 **Californian Upwelling System (CaUS)**

118 In the Californian system, the strongest wind stress takes place in spring in the southern portion of the  
119 CaUS. In summer the strongest winds occur offshore of northern California around 38° N. This wind  
120 stress pattern diminishes as we move away from this latitude in both directions (Bakun and Nelson, 1991).  
121 Among the four regions depicted by Kämpf and Chapman (2016), the strongest upwelling occurs in two  
122 well-known upwelling centers that we have selected for the analysis in this study: Cape Mendocino  
123 (Abbott and Zion, 1987) and Point Conception (Dugdale and Wilkerson, 1989), south of it, the wind's  
124 seasonal variability is different.

### 125 **Canarian Upwelling System (CanUS)**

126 Following Kämpf and Chapman (2016), the CanUS is divided into two distinct upwelling areas, which  
127 experience limited continuity of flows between them. This division arises due to the coastline interruption  
128 in the Strait of Gibraltar that leads to two upwelling areas: the Iberian Upwelling System and the Canarian  
129 Upwelling System. Given the lack of permanent upwelling centers in the Iberian Upwelling System, we  
130 have focused on the Canarian Upwelling System. Following Cropper et al. (2014), we selected the two  
131 upwelling centers (UP1 and UP2) on the cold SST cores (see Fig 2b) within the permanent upwelling  
132 area.

### 133 **Humboldt Upwelling System (HuUS)**

134 The HuUS is characterized by prominently strong upwelling zones along the Peruvian-Chilean coastline,  
135 due to the topographical influence of headlands, as described by Figueroa & Moffat, (2000) and Mesias  
136 et al., (2003). Notable regional upwelling centers encompass the continental shelf near Pisco (13.7° S),  
137 Antofagasta (21-25° S), and the Mejillones Peninsula (23° S), as well as extending further south to  
138 Coquimbo Bay (30° S), Valparaíso (33° S), and the Bay of Concepción (37° S). Moreover, in the  
139 Mejillones Peninsula (23° S), both observational (e.g., Marín, 2003) and modeling studies (Escribano et

140 al., 2004) have revealed that the dynamics of coastal ecosystems in this area heavily rely on the generation  
141 of upwelling filaments. Additionally, the continental shelf near Pisco (13.7° S) emerges as an  
142 exceptionally productive and distinctive upwelling center. Hence, the two upwelling centers selected are  
143 the Mejillones Peninsula and Pisco.

#### 144 **Benguela Upwelling System (BeUS)**

145 As Kämpf and Chapman (2016) described, within the Benguela Upwelling System, numerous upwelling  
146 centers extend along the shelf area of the Benguela Current region. These centers include Cape Frio (18.5°  
147 S), Walvis Bay (22.95° S), Lüderitz (26.45° S), Namaqualand (28.55° S), Cape Columbine (32.85° S),  
148 and Cape Town (33.95° S). Lüderitz stands out as a particularly noteworthy upwelling center within this  
149 system (Andrews and Hutchings, 1980; Lutjeharms and Meeuwis, 1987; Peard, 2007). As Hutchings et  
150 al. (2009) defined, Lüderitz represents an intensive perennial upwelling center characterized by intense  
151 winds, high turbulence, and robust offshore transport. Another significant area of interest lies in Cape  
152 Columbine, primarily due to its biological importance (Andrews and Hutchings, 1980; Bang and  
153 Andrews, 1974; Andrews and Cram, 1969). Given these distinctive features, we have selected Lüderitz  
154 and Cape Columbine as the upwelling centers for our analysis.

#### 155 **3.2. Trends Analysis**

156 With a minimum data length (>30 years), a climate series can usually be described as a combination of  
157 multiple variabilities at different time scales. Since we are interested in the trend of the record, we  
158 removed the high-frequency variability (<1 yr) by averaging the daily NOAA SST analyses data (1982-  
159 2021) into monthly means and removing the seasonal cycle. The seasonal cycle is a recursive signal  
160 throughout the entire record, and therefore, it does not influence the trend but induces noise in the target  
161 scale. The monthly climatology was subtracted from the record to remove the seasonal cycle. After this  
162 pre-analysis, we calculated the trend with the ordinary least square method. We evaluated the strength of  
163 these correlations using the Pearson Correlation Coefficient (PCC). The following qualitative  
164 classification will be used throughout the manuscript: Perfect (1), very high (>0.9), high (>0.7), and  
165 moderate (>0.5). Additionally, we employed the simple Mann-Kendall (MK) test to evaluate the statistical

166 robustness (Kendall, 1975; Mann, 1945). The MK tests verify whether an n-length series holds a  
 167 monotonic increase or decrease trend. In addition, we need to consider the instrumental error since,  
 168 historically, a warm coastal bias is found in satellite records compared to in-situ records (Smale and  
 169 Wernberg, 2009). This bias was assessed in the northern hemisphere by validating the data using in-situ  
 170 observations. Additionally, to assess the drivers of change in upwelling intensity, we calculated the sea  
 171 level pressure (SLP) gradients for each EBUS. The gradients were calculated between the cores of the  
 172 high- and low-pressure systems (exact positions provided in supplementary material, Fig S1). To  
 173 corroborate the Rykaczewski hypothesis, we used the spatial standard deviation. A displacement of the  
 174 pressure systems would increase the standard deviation of the trends around their cores.

### 175 3.3. Angular Index of Upwelling Intensification ( $\alpha_{UI}$ )

176 To test Bakun's hypothesis, a new index, named the Angular Index of Upwelling Intensification ( $\alpha_{UI}$ ), is  
 177 proposed. This new index uses the angle between the trend of the most robust upwelling cell at each  
 178 EBUS and the trend at the corresponding open ocean area. If the upwelling intensifies, as Bakun proposed,  
 179 the trends in the open ocean and the cell are expected to differ significantly, resulting in a higher angle  
 180 between the trends. To calculate  $\alpha_{UI}$ , two vectors (in the time-temperature space) may be constructed from  
 181 the upwelling ( $\overline{Up}$ ) and oceanic ( $\overline{Oc}$ ) trends. The rotation sense (clockwise or anticlockwise) is used to  
 182 calculate the relative orientation of ( $\overline{Up}$ ) over ( $\overline{Oc}$ ), needing to consider an additional unit vector ( $\overline{n}$ )  
 183 normal to  $\overline{Up}$  and  $\overline{Oc}$

184 The mathematical formulation of  $\alpha_{UI}$  is

$$185 \quad \alpha_{UI} = \arctan^* \left( \frac{((\overline{Up} \times \overline{Oc}) \cdot \overline{n})}{\overline{Up} \cdot \overline{Oc}} \right) = \arctan \left( \frac{|\overline{Up}| |\overline{Oc}| \sin(\alpha_{UI})}{|\overline{Up}| |\overline{Oc}| \cos(\alpha_{UI})} |\overline{n}| \cos(\beta) \right)$$

186 \* We used the four-quadrants arc tangent in this analysis since it allows to determine the sign of the  
 187 angle based on the signs of the arguments.

188 Following the right-hand rule, if the cross product of ( $\overline{Up}$ ) and ( $\overline{Oc}$ ) is anticlockwise (that is, if the open  
 189 ocean trend ( $\overline{Oc}$ ) is greater than the upwelling trend ( $\overline{Up}$ ), the resulting vector of the cross product has the  
 190 same orientation as  $\overline{n}$ . This implies that the dot product ( $\overline{Up}$ )  $\times$  ( $\overline{Oc}$ )  $\cdot \overline{n}$  is positive since the angle ( $\beta$ )  
 191 between  $\overline{n}$  and ( $\overline{Up}$   $\times$   $\overline{Oc}$ ) is 0°. In case the upwelling trend is greater than the open ocean trend,  $\overline{Up}$   $\times$   $\overline{Oc}$



192 results negative since  $\beta$  is now  $180^\circ$ . Note that this methodology is susceptible to the order of the vectors,  
193 as  $\overline{Up} \times \overline{Oc} = -\overline{Oc} \times \overline{Up}$ . Since we are interested in the relative position of the upwelling trend concerning  
194 the oceanic waters, the order used is  $\overline{Up} \times \overline{Oc}$ . It is important to note that the angle derived from  
195 trigonometric functions are not influence by units associated with the original vectors. Therefore, this  
196 new index is independent of temperature and time units.

197 We also conducted a probabilistic assessment of uncertainties for  $\alpha_{UI}$ , taking into account the uncertainties  
198 associated with upwelling and open ocean SST series. We performed an error estimation using the Monte  
199 Carlo method: individual data points were separately and randomly sampled 10,000 times within their  
200 respective  $(Up)^-$  and  $(Oc)^-$  uncertainty ranges. These new sampled series were then used to calculate  
201  $\alpha_{UI}$ . The standard deviation of the 10,000 simulations represents the uncertainty of  $\alpha_{UI}$ .

### 202 3.4. Satellite Validation

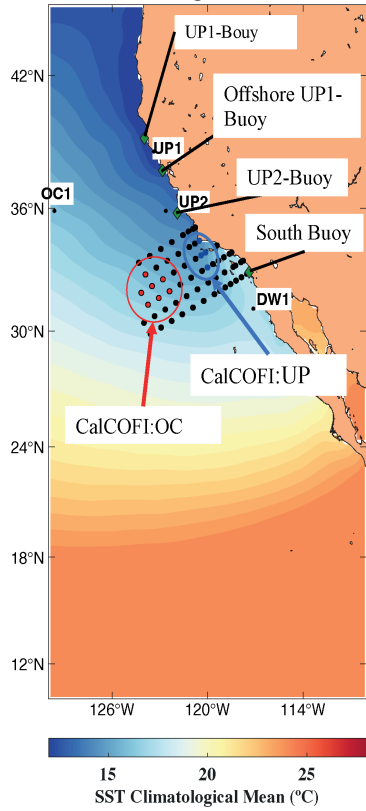
203 Taking advantage of the in-situ observations available in the study areas defined in Fig 2, we performed  
204 a validation through linear regression between in-situ and the deseasonalized satellite data. Records with  
205 no systematic error correspond to a linear regression slope with a value of 1 (perfect). Since the Pacific  
206 Ocean is better sampled than the Atlantic, better reanalysis performance and higher correlation are  
207 expected in the Pacific Ocean.

## 208 4. Results

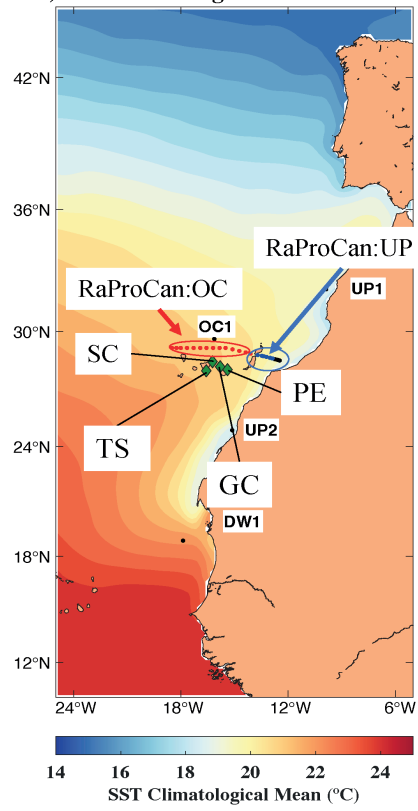
### 209 4.1. Satellite Validation

210 We first carried out a regional validation, in the northern hemisphere, with in-situ observations (Fig 2a  
211 and 2b) to test the consistency of the NOAA SST analyses between oceans. A linear fit between in-situ  
212 and satellite data gives insights into the reliability of the SST data in both oceans. As described in Section  
213 2, the in-situ dataset was divided into two categories: mooring and cruise data. Because each record has  
214 a different spatial and temporal resolution, categories are not comparable.

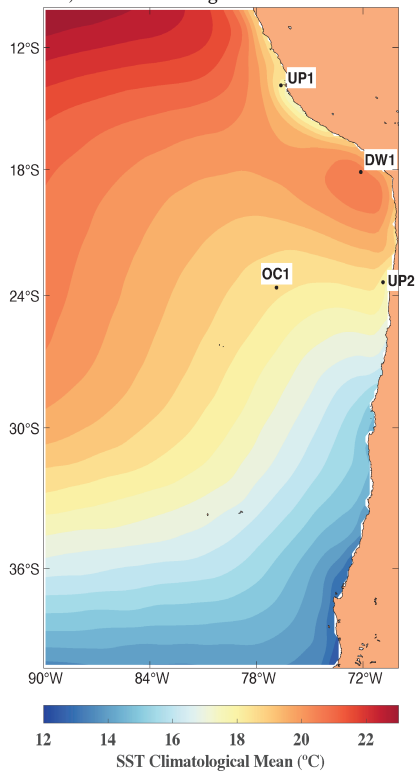
a) SST climatological mean of CalUS



b) SST climatological mean of CanUS



c) SST climatological mean of HuUS



d) SST climatological mean of BeUS

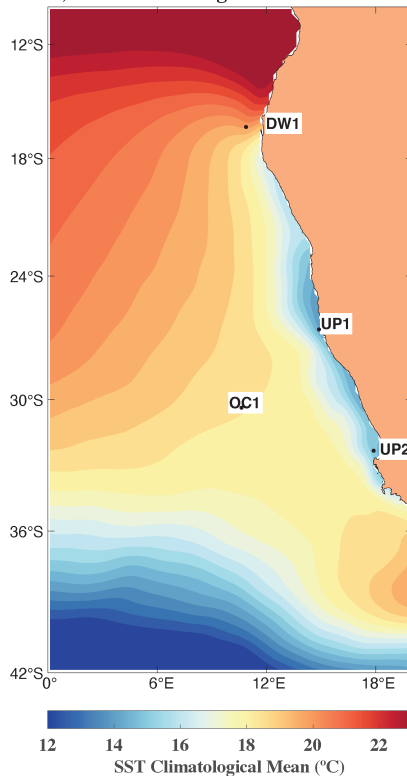


**Fig 2: Average SST maps for each of the Upwelling Systems: CalUS (a), CanUS (b), HuUS (c), and BeUS (d). Overlaid are the locations of the moorings (green diamond) and cruise data (black dots) used for the satellite validation with their corresponding names. The cruise stations were divided into upwelling and open ocean areas marked with blue and red circles, respectively. The representative points of UP, DW, and OC in each basin are shown as black dots.**

215 In the Pacific Ocean, the moorings selected were those as close as possible to the areas UP1, UP2, DW1,  
216 and OC1 described in section 3.1 and 3.4. We found the highest correlations inside the upwelling center  
217 of this region, where the UP1-Buoy and UP2-Buoy presented a linear regression fit of 0.99, supported by  
218 a very high correlation strength (0.94 and 0.92, respectively, Table 1). In the area where the upwelling  
219 meets the oceanographic background, the correlation of the offshore UP1-Buoy with the NOAA SST data  
220 decays slightly, presenting a linear slope of 0.84 and a correlation strength of 0.86. For the South-Buoy,  
221 close to DW1, the lineal fit and correlation (0.97 and 0.92) are closer to the values inside of the upwelling  
222 cell than of the offshore UP1-Buoy (Table 1). The results obtained for the offshore UP1-Buoy exemplify  
223 the effect of using an average large area surrounding the upwelling centers instead of a point, as the  
224 average introduces noise by adding points where upwelling might not be taking place, reducing the  
225 correlation in the transitional zone.

226 The cruise observations in the Pacific Ocean (CalCOFI) were divided into two different areas, open ocean  
227 (CalCOFI: OC) and upwelling (CalCOFI: UP), and we avoid data at transitional areas, as seen in Fig 2a.  
228 The results of the linear fit between the cruise and the reanalysis data are similar to those obtained with  
229 the mooring data (Table 1 and supplementary material Fig S2). The average within the upwelling cell,  
230 CalCOFI: UP, has a very high linear regression value (0.91), while for the offshore stations, CalCOFI:  
231 OC, the regression is 0.81. Nevertheless, the strength of the correlation is sensitive to the amount of data  
232 available from the cruise data in the ocean versus the upwelling areas. Additionally, due to the time  
233 resolution of the cruise, the correlation strength is moderate (0.68) for the CalCOFI: OC and high (0.71)  
234 for the CalCOFI: UP.

235 We also compared the EN4 dataset (Table 1, two last columns) against the NOAA SST analysis. As  
236 described in section 2, due to the coarse temporal resolution of the cruise data, it was not possible to  
237 compare with the EN4 monthly. Overall, the EN4 has lower correlation and regression values than the  
238 NOAA SST analyses. The correlation has the same pattern in both datasets (NOAA and EN4): moderate

239 in the northern locations (0.60 and 0.63) and high in the southern locations (both with 0.76), although the  
 240 data length of the EN4, unlike the cruise records, is the same as the mooring.

<b>In-situ Data</b>	<b>NOAA</b>		<b>EN4</b>	
	Linear Slope	Correlation	Linear Slope	Correlation
UP1-Buoy (46014).	0.99	0.92	0.70	0.60
Offshore UP1-Buoy (46028).	0.84	0.86	0.72	0.63
UP2-Buoy (46225).	0.99	0.94	0.78	0.76
South-Buoy (46026).	0.97	0.92	0.77	0.76
CalCOFI: OC	0.81	0.71	-	-
CalCOFI: UP	0.91	0.68	-	-

241 **Table 1. Values of the linear regression and Pearson's correlation strength between the in-situ data (listed in the**  
 242 **first column, with the designation within the manuscript and, in brackets, the official NDBC station ID). The in-**  
 243 **situ data are compared with the NOAA SST reanalysis (second and third columns) and the EN4 product (last two**  
 244 **columns) validation for the Pacific Ocean. The last two rows are for the CALCOFI cruise data of the Pacific**  
 245 **Ocean.**

246 In the Atlantic Ocean, the number of in-situ measurements available is more limited than in the Pacific  
 247 Ocean. Therefore, the long-term records are shorter than in the Pacific Ocean and are only available in  
 248 the surroundings of the Canary Islands. The results reflect these limitations since none of the linear  
 249 regressions or correlation coefficients ever exceeds 0.9, unlike the results for the Pacific Ocean (Table 1).  
 250 As in the Pacific Ocean, the mooring data shows a better linear regression and higher correlation  
 251 coefficient than the cruise data (Table 2 and supplementary material, Fig S3). The correlation coefficients  
 252 for the buoys of Santa Cruz, Gran Canaria, and Tenerife Sur are high, with values of 0.89 (0.84), 0.84  
 253 (0.87), and 0.83 (0.88), respectively. The result of Las Palmas East-Buoy is comparable to the linear slope  
 254 for the cruise data, 0.71. However, the Las Palmas East-Buoy has a higher correlation coefficient (0.89),  
 255 which agrees with the other moorings.

256 For the cruise data, we follow the same approach as in the Pacific Ocean, dividing the data into open  
 257 ocean areas (RaProCan: OC) and upwelling centers (RaProCan: UP). As occurred for the results in the  
 258 Pacific, the regression is better for the upwelling cell with values of 0.73 and a correlation strength of  
 259 0.71. For the open ocean areas (RaProCan: OC), the linear slope is slightly lower (0.63) but has a higher  
 260 correlation strength coefficient (0.77).

261 The EN4 dataset was also used in these areas and showed linear regressions and correlation coefficients  
 262 similar to the cruise data, as shown in Table 1. In Table 2, the linear regressions of EN4 are close to the  
 263 results of the moorings, even though EN4 performs similarly compared to Table 1. Thus, EN4 seems a  
 264 better alternative in the Atlantic Ocean than in the Pacific Ocean, but only due to the lower performance  
 265 of the NOAA SST analyses in the Atlantic Ocean. However, the correlation strength of the EN4 showed  
 266 lower values than NOAA SST analyses, with three out of five locations under 0.70. Hence, using the  
 267 NOAA SST analyses for long-term analysis in both oceans is a better approach.

<b>In-situ Data</b>	<b>NOAA</b>		<b>EN4</b>	
	Linear slope	Correlation	Linear Slope	Correlation
Las Palmas East Buoy.	0.71	0.89	0.80	0.71
Santa Cruz Buoy.	0.89	0.84	0.71	0.66
Gran Canaria Buoy.	0.84	0.87	0.76	0.54
Tenerife South Buoy.	0.83	0.88	0.77	0.53
RaProCan: OC	0.63	0.77	-	-
RaProCan: UP	0.73	0.71	-	-

268 **Table 2. Values of the linear fit and correlation strength between in-situ data (listed in the first column) and both**  
 269 **the NOAA SST analyses (second and third columns) and the EN4 product (last two columns) for the Atlantic**  
 270 **Ocean. The last two rows are for the RaProCan cruise data of the Atlantic Ocean.**

#### 271 4.2. Trend patterns on the EBUS

272 We begin by identifying the overall pattern of the long-term trends in each EBUS, which we show in Fig  
 273 3. A general pattern of cooling (negative) trends within the upwelling centers and warming (positive)  
 274 trends offshore is found in most of the regions. An exception is found in the HuUS, where there is also a  
 275 cooling trend offshore. This cooling mode, however, is not as pronounced as the trends onshore driven  
 276 by the upwelling process. On top of these general patterns, each region presents unique features that will  
 277 be described in the following paragraphs.

278 The mean trend for the CalUS (Fig 3a) is 0.10 (SD= 0.06) °C/decade. The minimum values, -0.17  
 279 °C/decade, are located near Cape Mendocino, around 43-39°N, and 32°N corresponding to the permanent  
 280 upwelling centers. On the other hand, maximum values (excluding the shallower Gulf of California),

281 reaching up to 0.20 °C/decade, are located south, at 30°N, where the winds are non-favorable for year-  
282 round upwelling, and there is convergence (Kämpf & Chapman, 2016). At around 22 °N, there is an  
283 offshore negative trend area with mean values of -0.02 °C/decade. However, the MK test revealed that  
284 these trends in the offshore area are not significant. The non-significant extensive regions in the MK test  
285 support the idea that the trends in the CalUS coastal upwelling are only statistically distinguishable from  
286 zero within the upwelling centers.

287 In the CanUS (Fig 3b), the mean trend in the region is warmer than in CalUS, with a value of 0.20 (SD=  
288 0.04) °C/decade. The minimum values (-0.20 °C/decade) are confined to two upwelling centers in the  
289 permanent annual upwelling zones, located north of Cape Ghir and south of Cape Bojador. The maximum  
290 warming trend is 0.60°C/decade, located west of Cape Timiris in the Mauritania-Senegalese convergence  
291 zone. Because of the low spatial variability of the trend in the CanUS, the mean offshore value is the same  
292 as the average value of the entire CanUS.

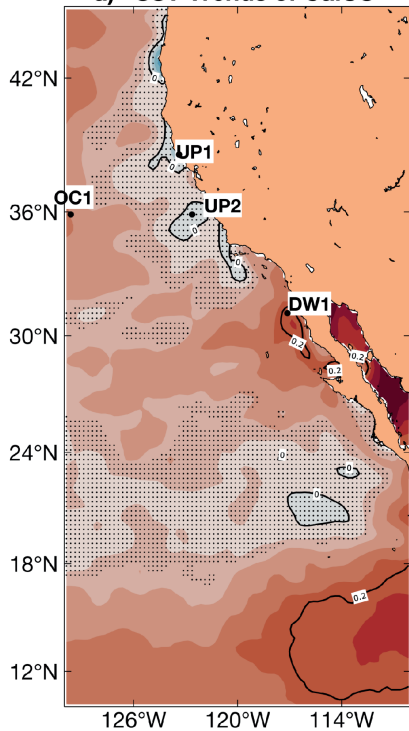
293 For the HuUS (Fig 3c), the mean value of the region is 0.007 (SD= 0.09) °C/decade. a cooling signal  
294 stands out as the general pattern in the tropic, with a mean value of -0.15 °C/decade. Despite this cooling  
295 of the overall trend, there are two clear upwelling centers, at 13°N and 24°N, with minimum values of -  
296 0.36 °C/decade. In these upwelling centers, the negative trends are lower than in the open ocean at the  
297 same latitudes.

298 Finally, in the BeUS (Fig 3d), the mean trend is 0.19 (SD= 0.09) °C/decade, closer to the average of the  
299 CanUS. The two warm fronts with trends over 0.40 °C/decade can be found in both the north and south  
300 ends. In the round-year upwelling area, the Lüderitz cell (Andrews and Hutchings, 1980; Lutjeharms and  
301 Meeuwis, 1987; Peard, 2007), the minimum value is -0.25 °C/decade. In contrast, for the open ocean area  
302 between the two warm fronts, the values are similar to those found in the CanUS (Fig 3b), around 0.20  
303 °C/decade.

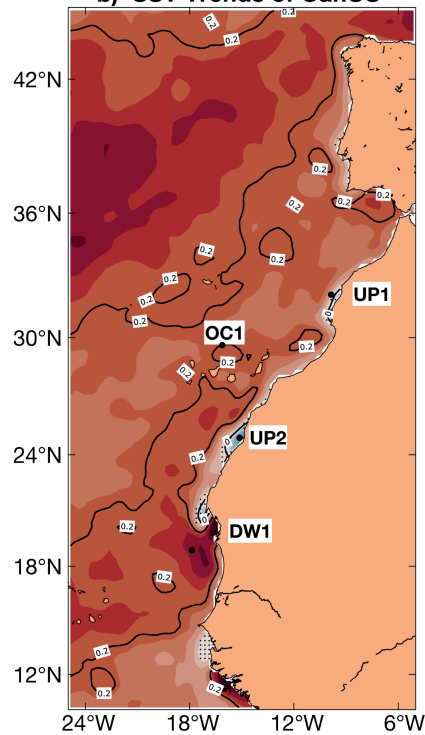
304 The average trend for each region reveals higher open ocean warmings for the Atlantic EBUS (0.20 and  
305 0.19 °C/decade for the CanUS and BeUS, respectively) than the Pacific Ocean (0.10 and 0.007 °C/decade,  
306 for the CalUS and HuUS, respectively), with the lower trends observed in the HuUS. However, the trends  
307 along the coast are rather heterogeneous, responding to the variability of the local upwelling dynamics,

308 as seen in Fig 3, where several permanent upwelling centers (negative trends) exist along the coast on  
309 both continents.

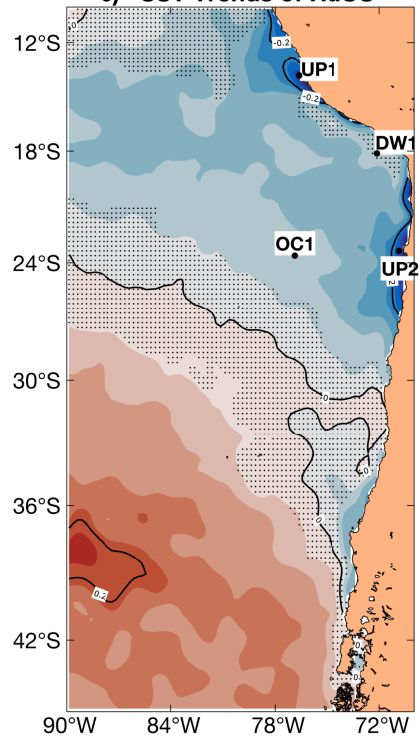
a) SST Trends of CalUS



b) SST Trends of CanUS



c) SST Trends of HuUS



d) SST Trends of BeUS

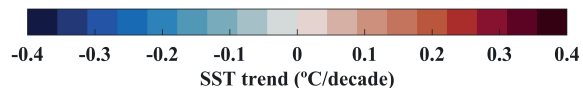
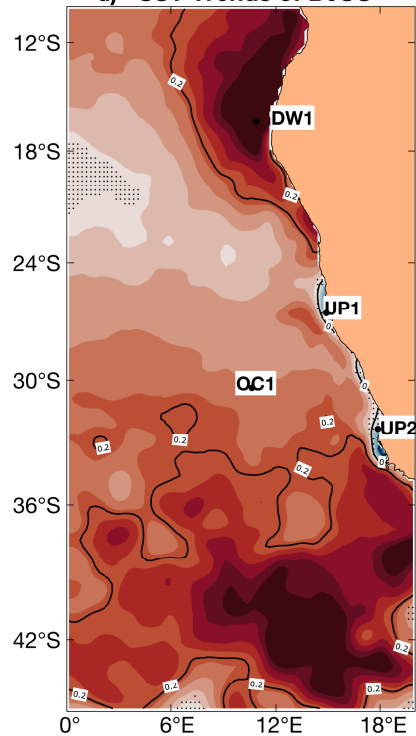




**Fig 3: Mapped SST trends (°C/decade) for the major EBUS: a) California -CalUS, b) Canary-CanUS, c) Humboldt-HuUS, and d) Benguela-BeUS. The color scale indicates the trend values at the right margin of each graph. Black-dots shaded areas indicate non-significant trends. The locations of the areas selected (UP1, UP2, OC1, and DW1) are marked with solid black circles and labelled with their names. Black contours enclosed the isotrends -0.20, 0, and 0.20°C/decade.**

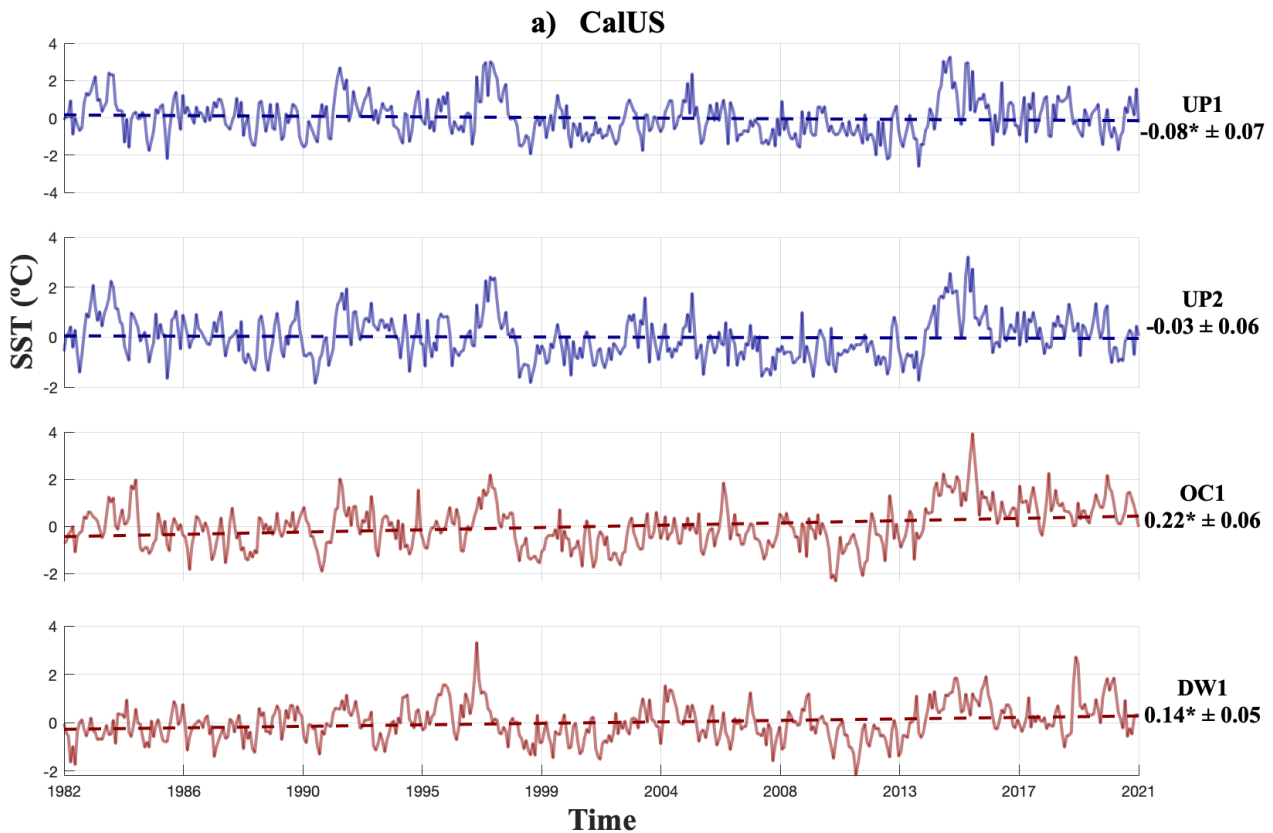
### 310 4.3. Trends in the upwelling cells and open ocean areas.

311 Although we got an overview of the long-term trends for each EBUS in the previous section, the  
312 validation of Bakun's hypothesis would require a finer resolution to describe the local dynamics of the  
313 upwelling and identify those areas where the coastal upwelling is the main forcing. In this sense, we have  
314 chosen representative points (see criteria in Section 3.4 and Figs 2 and 3) of both EBUS and non-EBUS  
315 areas instead of using the large-averaged regions shown in Fig 3. These upwelling points are the upwelling  
316 centers (UP1, UP2), the nearshore areas where the upwelling is not the primary process (DW1), and the  
317 open ocean areas (OC1).

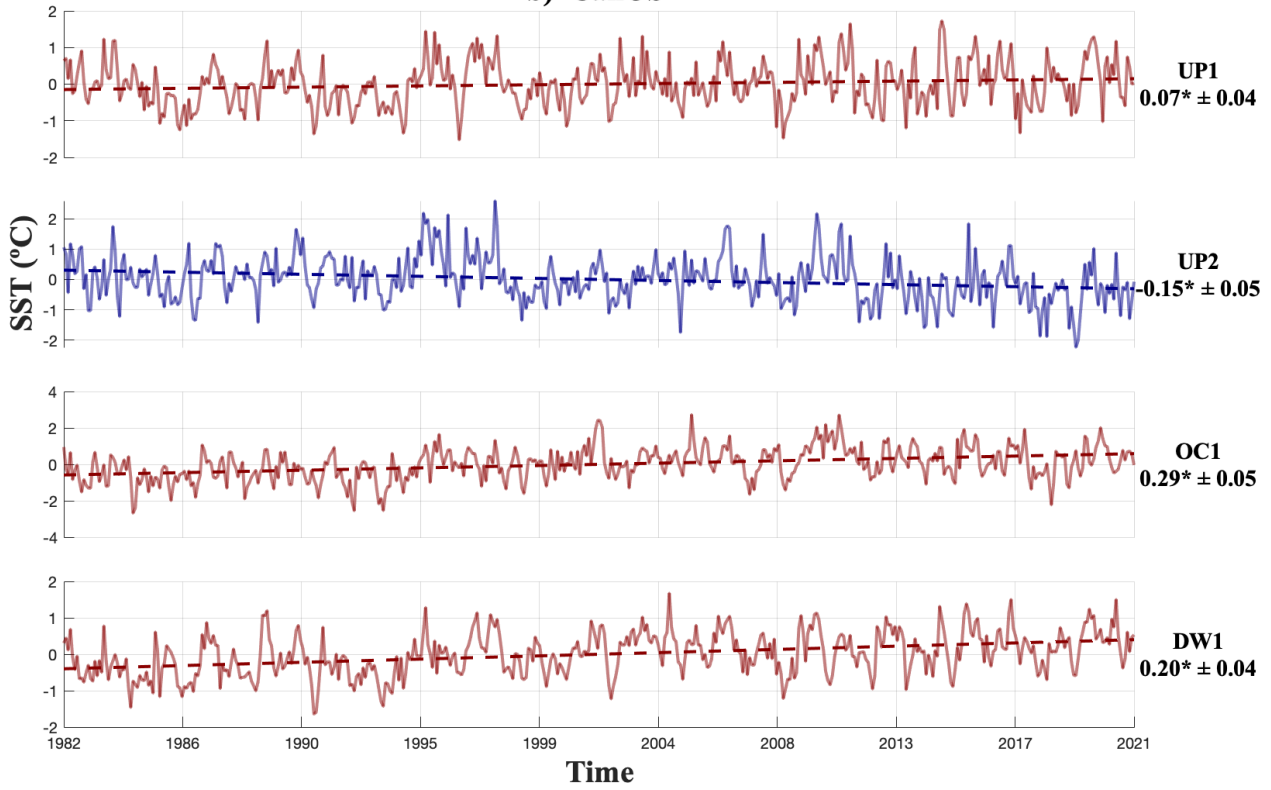
318 The CalUS presents the weakest trends of all the EBUS in both year-round upwelling centers, being -0.06  
319 °C/decade for UP1 and non-significant in UP2 ( -0.03 °C/decade, Fig 4a). For the open ocean area, the  
320 OC1 trend is positive with a value of 0.14 °C/decade, a lower value than the trend of 0.22° C/decade of  
321 the DW1. On the Atlantic, the CanUS (Fig 4b) possesses the only positive trend (0.07 °C/decade) of all  
322 the EBUS in an upwelling area (UP1). Despite UP1 being positive, the trend is closer to zero than in the  
323 OC1 (0.20 °C/decade). Furthermore, the UP2 cell in the CanUS shows a trend twice as negative (-0.15  
324 °C/decade) as the one on the CalUS upwelling UP1. The OC1 and DW1 areas show a warmer trend in the  
325 CanUS than in the North Pacific region (Fig 4). All of the above suggests that on the Northern Hemisphere  
326 EBUS, Bakun's hypothesis is fulfilled, and this is even more significant in the CanUS despite having been  
327 dismissed in previous studies (Sydeman et al., 2014).

328 In the HuUS (Fig 4c), we find a different behavior than the one seen on the other EBUS, showing negative  
329 trends in all the representative locations. The upwelling centers of the HuUS present the greatest cooling  
330 trend of all the EBUS, -0.30 °C/decade at UP1 and -0.26 °C/decade at UP2. As observed in CanUS, the  
331 values for HuUS in OC1 (0.06 °C/decade) are similar to the ones of DW1, although DW1 is non-  
332 significant in the HuUS. Its counterpart in the Atlantic Ocean, the BeUS (Fig 3d), presents significant  
333 large negative trends in the year-round upwelling areas (-0.23 °C/decade for UP1 and -0.10 °C/decade for

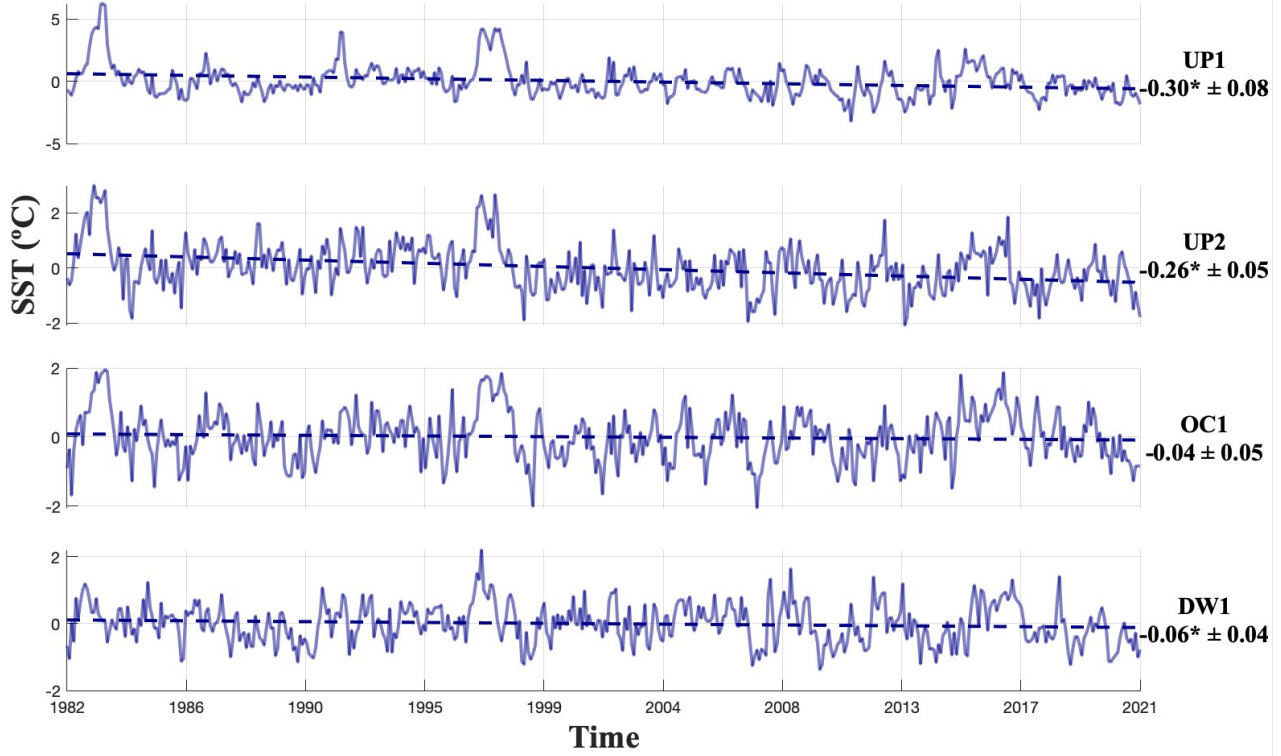
334 the UP2) and positive trends in OC1, 0.14 °C/decade. The trend of the DW1 is the warmest (0.57  
335 °C/decade) found in all the EBUS, and it is related to the warm inflow from the Indian Ocean.  
336 Overall, the trends show warming in the OC1 areas while cooling in the upwelling areas, except for the  
337 HuUS, where the trend at the OC1 is also slightly negative. The contrast between the trends of upwelling  
338 and open ocean areas found throughout the EBUS indicates upwelling intensification. To quantify this  
339 intensification, it is necessary to have an index that compares the intensification of the upwelling with the  
340 global warming trend on the open ocean area, that can be compared for all the EBUS. To compare the  
341 intensification between upwellings and to further understand the impact of the oceanic background on  
342 these trends, we will use the index  $\alpha_{UI}$  described before to normalize the trends of each EBUS.



**b) CanUS**



**c) HuUS**



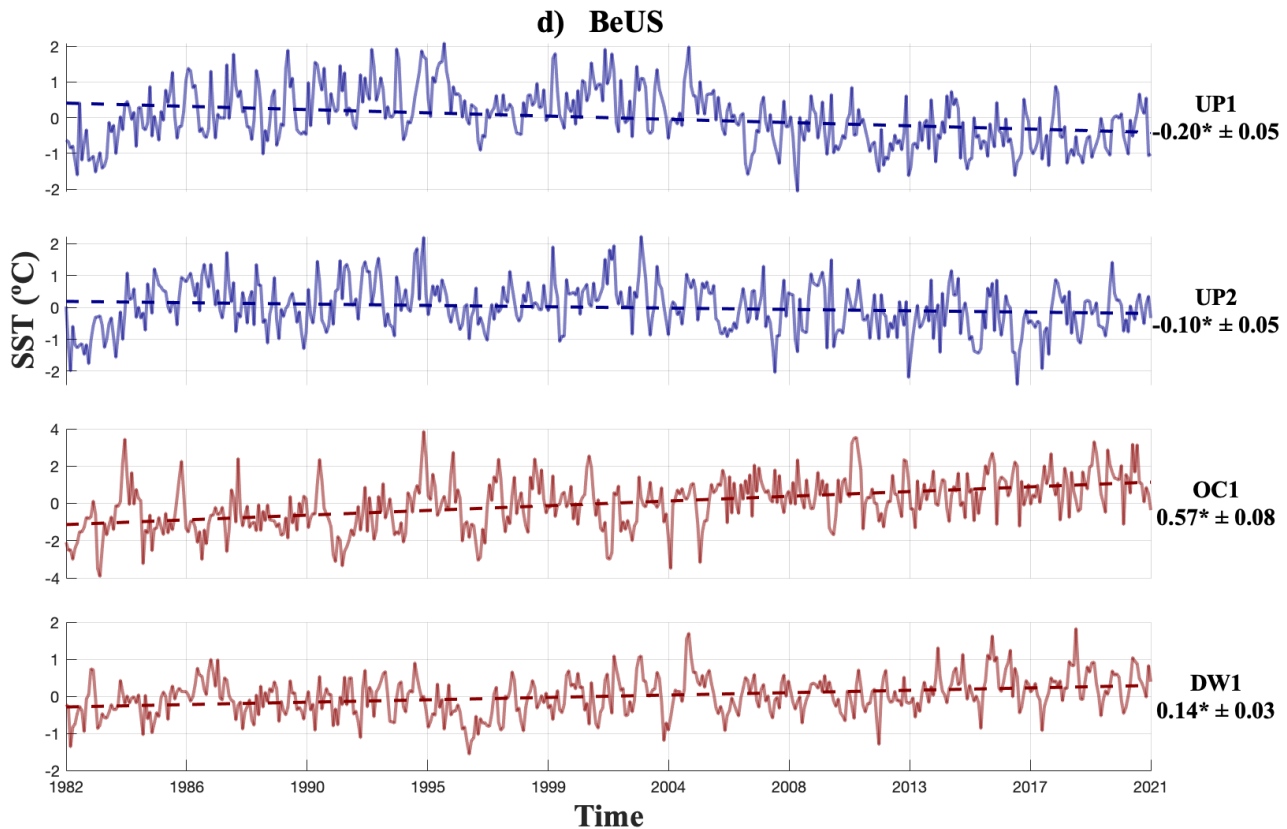


**Fig 4: SST time series and trends (°C/decade) for the selected areas for each one of the EBUS (DW1, UP1, and UP2) and the areas representative of the open ocean (OC1) in each EBUS: a) California, b) Canary, c) Humboldt and d) Benguela. The blue lines are for negative (cooling) trends, and the red ones are for positive (warming) trends. On the right side of the Y-axis, the trends are shown in °C/decade, along with the area's label and confidence interval. Mann-Kendall significant trends ( $p$ -value $<0.05$ ) are resalted with the symbol "\*" next to their value.**

343 **4.4. The relation between Oceanic and EBUS trends.**

344 Global warming induces the increase of oceanic SST, and under Bakun's hypothesis, it also enhances the  
 345 favorable upwelling winds responsible for intensifying the upwelling areas. We define an angle between  
 346 the upwelling and oceanic trends, as described in the methodology section, to discern Bakun's hypothesis  
 347 from the global increase in SST. As described previously (Fig 4), the upwelling centers UP1 (except for  
 348 the CanUS, where UP2 will be used due to the warming detected on UP1 in Section 4.3) have the strongest

349 cooling, and we will use these trends (hereafter, in this section UP) to create the angle contrasts with the  
350 positive warming trend of the open ocean (OC1) area for each EBUS (Fig 4).

351 For CanUS, the  $\alpha_{UI}$  obtained between the UP and OC1 trends is  $20^\circ \pm 2^\circ$  whereas it is  $11^\circ \pm 3^\circ$  in the CalUS,  
352  $21^\circ \pm 2^\circ$  for the BeUS, and  $14^\circ \pm 3^\circ$  for the HuUS. The smallest angle is found in the CalUS because of the  
353 low cooling and warming trends described in Section 4.3. This result for the CalUS is coherent with the  
354 overall non-significant trends in the Mann-Kendall test (Fig 3a). The BeUS and CanUS have the highest  
355 contrast between the two regression lines (recall that we observed similar UP and OC1 trends in the  
356 Atlantic Ocean in Section 4.3) presenting similar  $\alpha_{UI}$ .

357 The BeUS and CanUS show a weaker negative trend than the HuUS, but the oceanic background at the  
358 HuUS leads to a smaller angle. At the HuUS, a negative SST trend is observed for the whole study area.  
359 The hypotheses existing suggest that this trend is led either by a stronger La Niña (Meehl et al., 2016) or  
360 related to the Southern Ocean SST changes (Kang et al., 2023b, a). Nevertheless, at the HuUS, we have  
361 the most prominent upwelling negative trend. However, when normalized with the open ocean trend, the  
362 Bakun's effect is reduced. In the annual upwelling series of CalUS and HuUS, there are two prominent  
363 peaks associated with El Niño appeared around 1983 and 1997.

364 In general, we found positive  $\alpha_{UI}$  for all the EBUS, supporting the intensification of the upwelling-oceanic  
365 gradient, as expected from Bakun's hypothesis.

## Upwelling cell vs Open Ocean

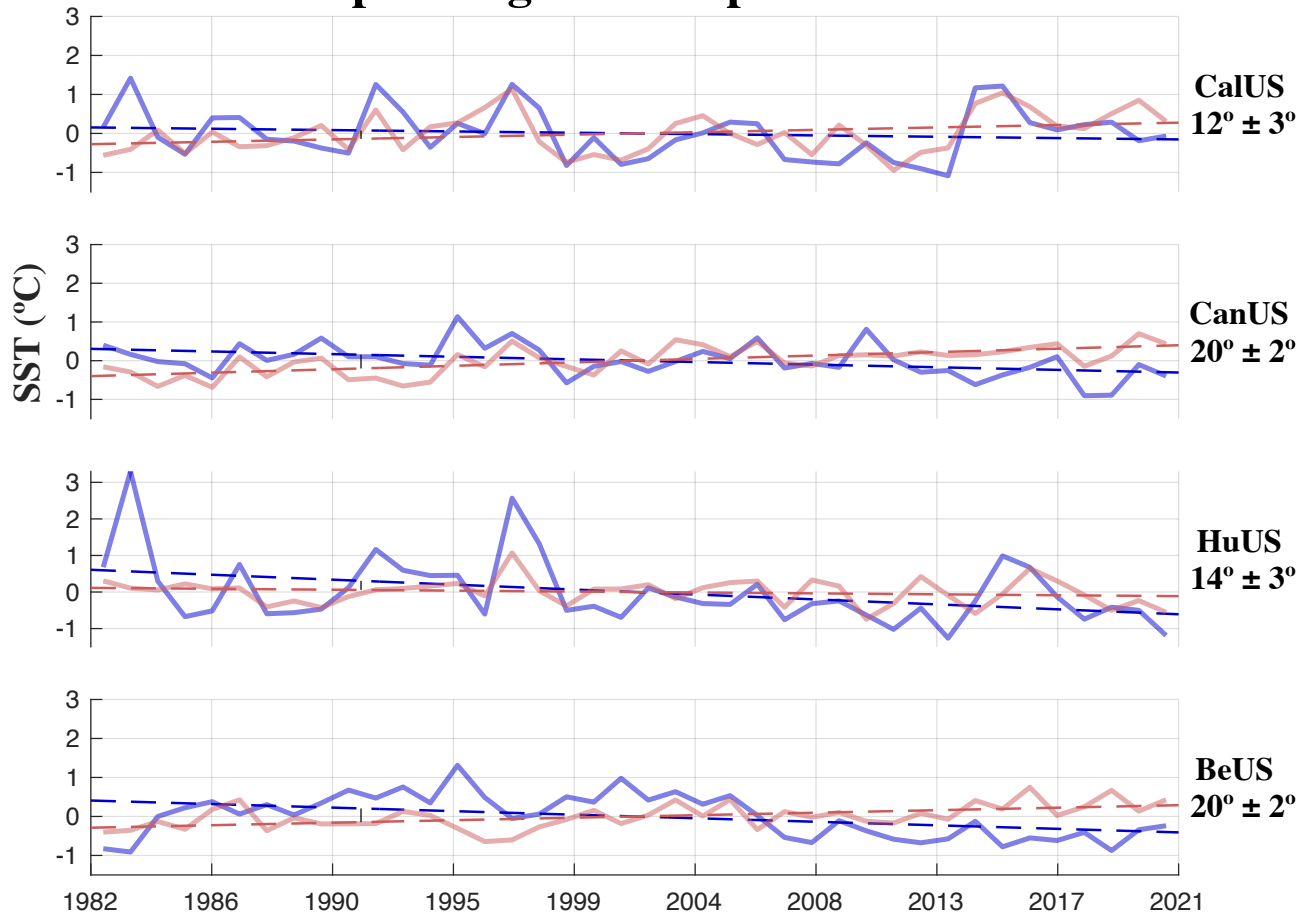


**Fig. 5: EBUS SST trends ( $^\circ\text{C}/\text{decade}$ ) against non-EBUS areas trends for each region. The EBUS annual series (continuous line) and trend (dotted line) are shown in blue; the same is true for the non-EBUS but is represented in red. On the opposite side of the Y-axis is labelled the  $\alpha_{UI}$  with their corresponding EBUS.**

366

### 367 4.5. Latitudinal distribution of $\alpha_{UI}$

368 Many authors have previously tested the Bakun hypothesis, providing little consensus on both historical  
 369 and projected records (Barton et al., 2013; Belkin, 2009; McGregor et al., 2007; Sambe et al., 2016, and  
 370 Sydeman et al, 2014;). Such controversy has yielded alternative hypotheses to explain changes observed  
 371 in the magnitude and timing of upwelling processes. Rykaczewski et al. (2015), suggests an alternative  
 372 mechanism to the intensification of the upwelling process. They suggest a poleward shift of the oceanic

373 high-pressure system which would stimulate latitude-dependent changes in the upwelling winds. To  
374 address this, we have calculated the latitudinal distribution of the  $\alpha_{UI}$  (see Fig 6) in each EBUS. The  
375 spatial variability of the upwelling intensity proxy,  $\alpha_{UI}$ , reveals distinct patterns and regional differences.  
376 In the CalUS, upwelling intensification demonstrates consistent upwelling activity between 35°N to 45°N  
377 with  $\alpha_{UI}$  values reaching up to approximately 10° (Fig 6a). Conversely, in the CanUS, significant  
378 upwelling intensification is observed between 20°N and 30°N, with  $\alpha_{UI}$  values peaking at 20° and in  
379 locations consistent with our dynamical analysis based on literature review (Fig 2b, UP1 and UP2).  
380 Similarly, in the HuUS upwelling intensification is confined to low latitudes (10-20 °S, Fig 6c), and the  
381 values are close to those of the CalUS, (index values around 10°), as seen in the previous section. In  
382 contrast with the other regions, the BeUS shows intensification at high latitudes with maximum values of  
383  $\alpha_{UI}$  (20°) in the upwelling center of this region – Lüderitz upwelling center at 25°S and Cape Columbine  
384 (around 32°S)-. While results of BenUS and CalUS appear consistent with the findings by Rykaczewski  
385 et al, (2015), there is no supportive evidence in the other regions. To elucidate the possible mechanism  
386 responsible for such differences we will attend to the driver of the favorable-upwelling wind, the sea level  
387 pressure gradient



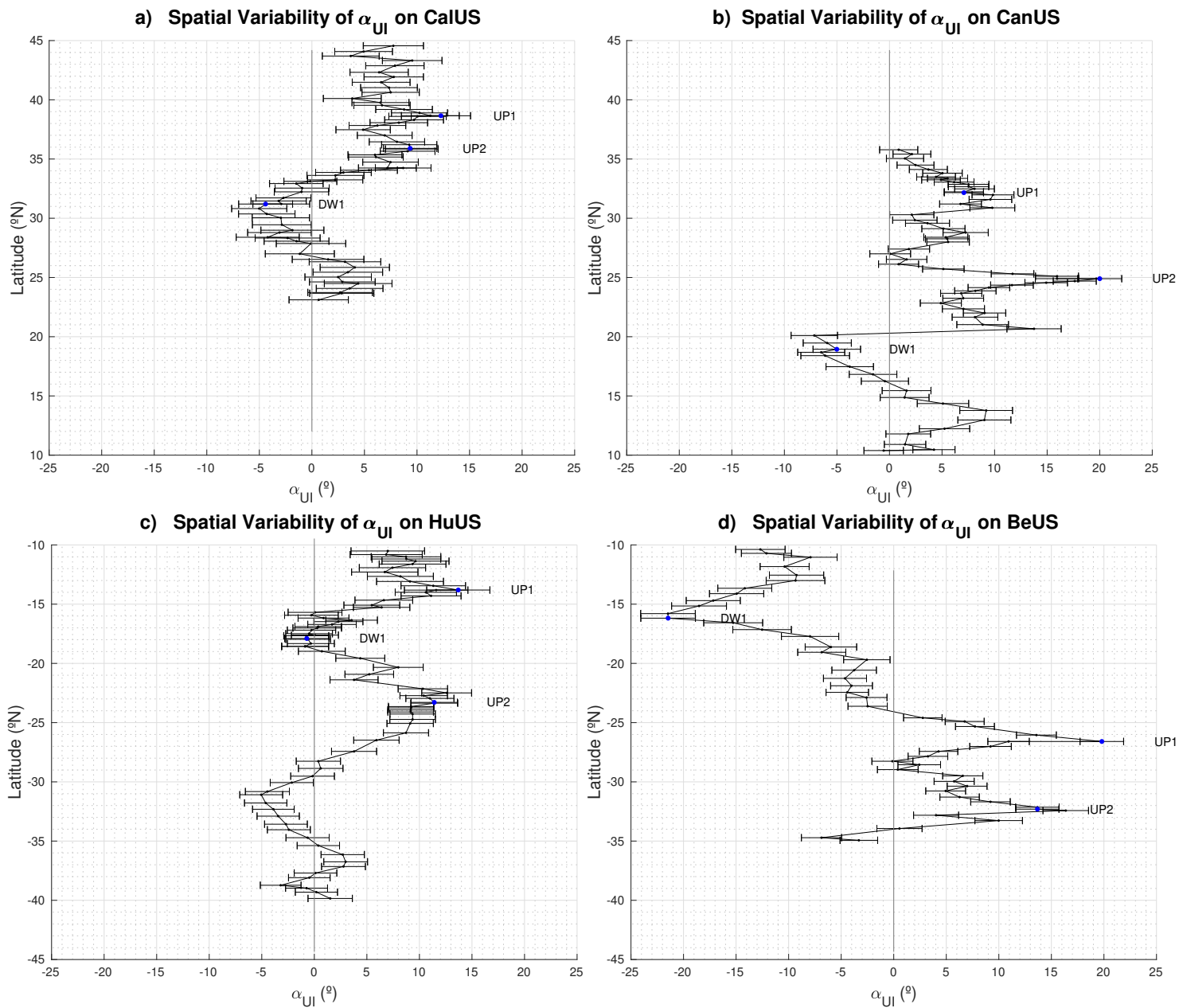


**Fig 6: Spatial distribution of the  $\alpha_{UI}$  (over the period of 1982-2021) along the coast for CalUS (a), CanUS (b), HuUS(c) and BeUS(c). The  $\alpha_{UI}$  is calculated between grid points along the coast and OC1.**

388 **4.6. SLP Gradients**

389 The coastal upwelling intensification postulated by Bakun mechanism, in 1990, would involve a stronger  
 390 increase of near-surface temperature over land than over the ocean, which would lead to an intensification  
 391 of the continental thermal low-pressure system relative to the ocean. To test this driver mechanism, we  
 392 have calculated the trends (Fig 7) of the gradient between the continental thermal low and the oceanic  
 393 high pressure.

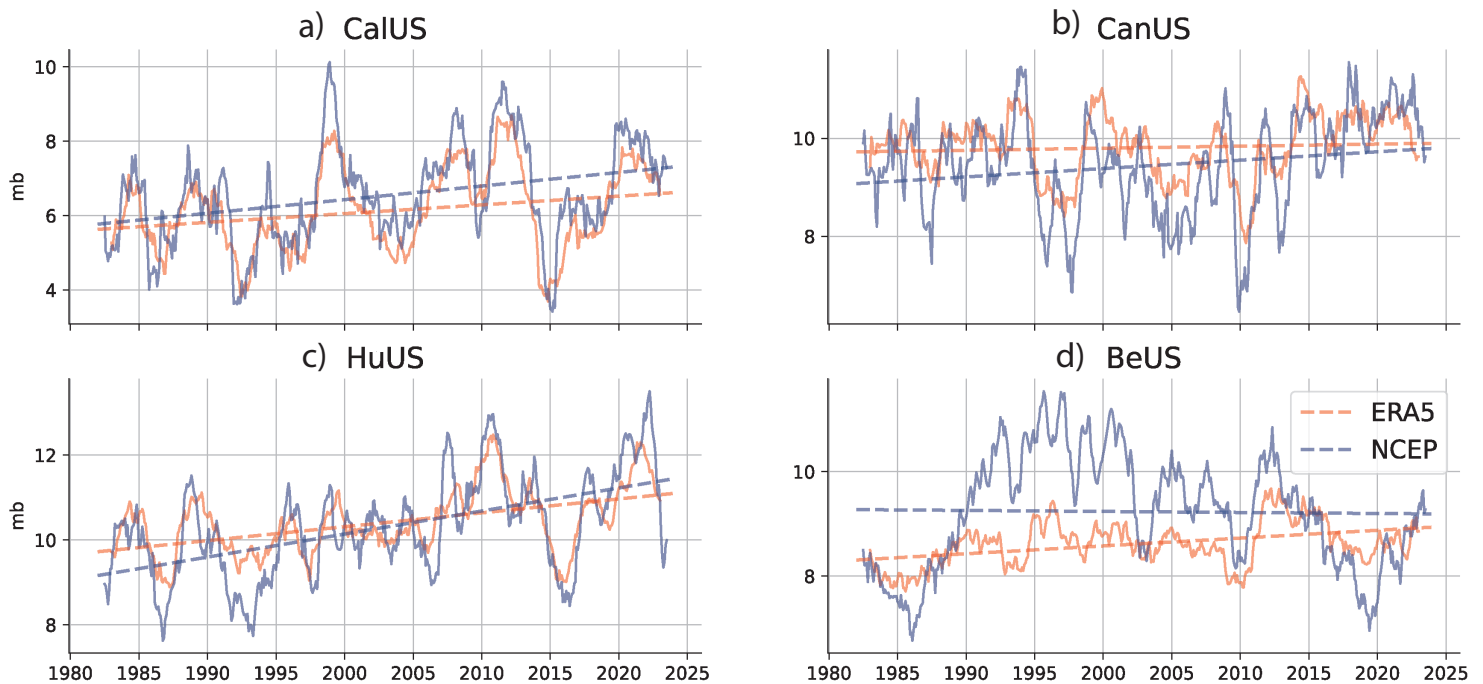


**Fig 7: EBUS SLP gradients trends and temporal series for NCEP (blue lines) and ERA5 (red lines) datasets over the period 1982- 2023.**

394 For ERA5, we found positive and significant trends (see Table 3) for all Eastern Boundary Upwelling  
 395 Systems (EBUS). Specifically, the trends in SLP gradients are 0.24 mb/decade (0.039) for CalUS, 0.04  
 396 mb/decade (0.017) for CanUS, 0.33 mb/decade (0.038) for HuUS, and 0.015 mb/decade (0.051) for  
 397 BeUS. On the other hand, the NCEP dataset shows no significant trend for the BeUS but stronger trends  
 398 than ERA5 for the other EBUS, with 0.37 mb/decade (0.073) for CalUS, 0.17 mb/decade (0.034) for  
 399 CanUS, 0.54 mb/decade (0.070) for HuUS, and -0.02 mb/decade (0.072) for BeUS. However, due to its

400 coarser resolution (2°) compared to ERA5 (0.25°), NCEP data is arguably less reliable. Nevertheless,  
 401 these results support an intensification of the pressure gradient.

	<b>CalUS (mb/decade)</b>	<b>CanUS (mb/ decade)</b>	<b>HuUS (mb/ decade)</b>	<b>BeUS (mb/ decade)</b>
<i>ERA5</i>	0.24 (0.039)	0.04 (0.017)	0.33 (0.038)	0.015 (0.051)
<i>NCEP</i>	0.37 (0.073)	0.17 (0.034)	0.54 (0.070)	-0.02 (0.072)

402 **Table 3. Values of the trend, over the period 1982-2023, for the ERA5 (first row) and NCEP (second row) for all**  
 403 **the EBUS. Parentheses enclose spatial standard deviation.**

#### 404 **5 Discussion and Conclusions.**

405 The future of the EBUS under global warming conditions remains uncertain. The controversies around  
 406 Bakun's hypothesis -an intensification of the upwelling due to the increase of the continental low-pressure  
 407 system driven by global warming- have its source in (1) discrepancies between wind stress datasets and  
 408 (2) differences in the methodologies used.

409 On one hand, Barton et al. (2013) highlighted a lack of consensus among various wind datasets, since  
 410 they did not observe statistically significant changes in the meridional (upwelling-favorable) wind. These  
 411 discrepancies in wind data are consistent with those noted by Narayan et al. (2010), who, despite finding  
 412 significantly increasing in coastal upwelling areas when using COADS wind stress, also found that the  
 413 NCEP/NCAR wind stress indicated a significant decrease in the upwelling off NW Africa, and a non-  
 414 statistically significant trend for Lüderitz, California, and the Peruvian upwelling areas. Furthermore, they  
 415 also observed that the ERA-40 dataset showed an increasing coastal upwelling in the NW African and  
 416 Peruvian upwelling areas but a decreasing in the California upwelling areas, with a non-statistically  
 417 significant trend in the Lüderitz upwelling areas Therefore, using wind data as a proxy for upwelling leads  
 418 to a wide spread of results as it strongly depends on the data product used.

419 On the other hand, SST-based indexes are usually constructed from thermal differences between coastal  
 420 and offshore SST areas taken at the same latitude and following the coastline (Benazzouz et al., 2014;  
 421 Gómez-Gesteira et al., 2008; Santos et al., 2012). This methodology does not consider the regional  
 422 upwelling dynamics, and average upwelling centers with areas without upwelling. Abrahams et al. (2021)  
 423 introduced an upwelling metric based on marine heatwave detection techniques, examining favorable

424 upwelling winds and SST data together. Their findings revealed a strong association between a decrease  
425 in SST and an increase in upwelling intensity. Their novel methodology holds significant importance in  
426 unraveling the connection between the physical upwelling phenomenon and its ecological impacts.  
427 However, predicting ecological impacts remains challenging. While intensified upwelling could mitigate  
428 habitat warming, it may also increase ocean acidification, hypoxic events and reduce suitable food for  
429 fish larvae (Abrahams et al., 2021; Bakun et al., 2015). Nonetheless, they successfully establish a link  
430 between decreased SST and changes in upwelling intensity, even when trends in wind dynamics do not  
431 fully account for the upwelling response, reinforcing the notion that SST is a suitable proxy for upwelling  
432 intensity. However, their SST metrics exhibited inconsistencies across upwelling areas, except for the  
433 Humboldt system. These inconsistencies may be due to the averaging of data across extensive areas,  
434 mixing upwelling areas with areas without the associated cold water of upwelling. Abrahams et al. (2021)  
435 also explored these metrics in upwelling-favorable winds data, and their results indicated that decadal  
436 trends were generally not significant. As previously discussed, wind products often yield contradictory  
437 results despite their direct relevance to upwelling. Hence, our study complements Abrahams et al. (2021)  
438 since we have focused on SST to understand longer terms changes in the upwelling intensity, using areas  
439 with optimal signal-to-noise ratio, namely the upwelling centers, revealing upwelling-related cool water  
440 in all Eastern Boundary Upwelling Systems (EBUS).

441 Therefore, in this study, we assess the intensification of the upwelling from a regional perspective, by  
442 using SST trends at locations representative of upwelling and of an open oceanic reference location for  
443 each different EBUS.

444 Additionally, we tested the effects of averaging areas on the index (see supplementary material, Fig S4  
445 and Table S1). Our findings indicate that the averaged response is influenced by the dynamical regions  
446 involved, rather than by the size of the region averaged. This is evidenced by the invariant results when  
447 including the three coastal areas (DW1, UP1 and UP2). In contrast, focusing on specific upwelling zones,  
448 particularly around upwelling centers, made the intensification more evident. Moreover, we verified the  
449 stability of the trend both spatially and temporally by performing the analysis of Barton et al. (2013)  
450 across all the EBUS (supplementary material, Fig S5).

451 Furthermore, to assess the strength of the net upwelling intensification, we proposed an index that allows  
452 inter-basin comparisons attending to their regional background. SST, often used as an indicator of coastal  
453 upwelling, can be influenced by various factors, such as changes in surface mixing and offshore storm  
454 activity. However, in our long-term analysis of monthly and deseasonalized SST records, the seasonal  
455 and synoptic processes have minimal influence on the SST-upwelling intensity relationship. Moreover,  
456 Wang et al. (2015) explored the connection between sea-land thermal gradients and offshore Ekman  
457 transport using the CMIP5 models. Their findings underscore the significant link between thermal  
458 gradients and offshore Ekman transport, even under greenhouse gas emission scenarios. McGregor et al.  
459 (2007) and Santos et al. (2012) also support this relationship, emphasizing significant correlations  
460 between coastal SST and offshore Ekman transport, reinforcing the utility of coastal SST as a proxy for  
461 assessing upwelling intensity.

462 To assess the quality of our results, we validated the NOAA SST reanalysis with in-situ data from both  
463 the Atlantic and Pacific Oceans before estimating the trends in all EBUS. Overall, the Atlantic Ocean had  
464 lower correlations with the satellite data than the Pacific Ocean, likely due to shorter in-situ records.  
465 Nevertheless, we found high and robust correlation coefficients ( $>0.7$ ) that sustain the satellite SST trends  
466 in oceanic and upwelling areas. We observed negative SST trends in all the EBUS, being stronger in the  
467 southern hemisphere (the strongest located in the HuUS-UP1 showing a  $-0.30^{\circ}\text{C}/\text{decade}$ ) than in the  
468 northern hemisphere (the weakest in the CalUS-UP2 with a trend of  $-0.06^{\circ}\text{C}/\text{decade}$ ). Our results are  
469 consistent with the meta-analysis by Sydeman et al. (2014), who concluded that a significant  
470 intensification of upwelling exists from observational and model data, except for the case of CanUS.

471 Other studies have investigated the SST trends in the EBUS but with an approach that did not consider  
472 the heterogeneity of the upwelling areas. For instance, in the CalUS, Seabra et al. (2019) reported a  
473  $0.06^{\circ}\text{C}/\text{decade}$  warming rate, over the period 1982–2018. However, their approach involved averaging a  
474 500 km nearshore area, excluding non-significant regions. Thus, almost half of the extension was not  
475 considered, resulting in the average of different dynamical areas and the exclusion of upwelling centers.  
476 Belkin et al. (2009) performed a similar analysis but included the entire CalUS nearshore area. They found  
477 a net change of  $-0.035^{\circ}\text{C}/\text{decade}$  over the 1982-2007 period, agreeing in sign with our study but showing  
478 a higher (more positive) rate due to the use of a large average. In contrast, Siemer et al. (2021) found

479 negative trends of  $-0.14^{\circ}\text{C}/\text{decade}$ , over the period 1982-2019, for the CanUS permanent upwelling area,  
480 like our results ( $-0.15^{\circ}\text{C}/\text{decade}$ ). However, this trend fades away and becomes positive when they  
481 average the whole coastal upwelling area, highlighting the relevance of the methodology used in this  
482 study. Likewise, many studies carried out in this area present positive trends for the upwelling due to the  
483 method used (Belkin, 2009; Demarcq, 2009; Seabra et al., 2019). In line with our study, Seabra et al.  
484 (2019) found the coolest trends ( $-0.07 \pm 0.08^{\circ}\text{C}/\text{decade}$ ) in the HuUS. However, like in other EBUS, using  
485 average areas increased the trend values. This pattern is also observed by Belkin et al. (2009), where the  
486 net change of the average nearshore area results in  $-0.05^{\circ}\text{C}/\text{decade}$ . For the BeUS, similar to CanUS,  
487 averaging the entire coastal upwelling area results in the fading of the observed upwelling trend. Hence,  
488 a warming rate of  $0.17^{\circ}\text{C}/\text{decade}$  is found in Seabra et al. (2019). In contrast, Santos et al. (2012)  
489 investigated trends, over the period 1982-2010, close to the shore without averaging areas and found a  
490 negative trend of the BeUS, strongly agreeing with our results ( $-0.13^{\circ}\text{C}/\text{decade}$ ). Hence, a warming rate  
491 of  $0.17^{\circ}\text{C}/\text{decade}$  is found in Seabra et al. (2019). In contrast, Santos et al. (2012) investigated trends  
492 close to the shore without averaging areas and found a negative trend of the BeUS, strongly agreeing with  
493 our results ( $-0.13^{\circ}\text{C}/\text{decade}$ ).

494 While all the upwelling trends are negative and support the Bakun's hypothesis, the oceanic trends behave  
495 differently across basins. We observed warming in all the open ocean areas except in the HuUS, where a  
496 cooling of  $-0.06^{\circ}\text{C}/\text{decade}$  is observed. Dong & Zhou (2014) studied the influence of the Interdecadal  
497 Pacific Oscillation (IPO) on Global Warming trends. Their EOF analysis results indicate that the transition  
498 to the negative phase of the IPO modes is responsible for the cooling trends observed in the Pacific.

499 The warming in the CalUS and BeUS is  $0.14^{\circ}\text{C}/\text{decade}$  (over the period 1982-2023), while this trend is  
500 slightly more prominent in the CanUS. Seabra et al. (2019) revealed oceanic warming rates  
501 ( $0.06^{\circ}\text{C}/\text{decade}$ ), over the period 1982–2018, on the averaged upwelling in CalUS lower than the OC1  
502 trend ( $0.14^{\circ}\text{C}/\text{decade}$ ). The open ocean positive trend of the CanUS is identical to the one in Siemer et al.  
503 (2021) and further agrees with other studies (Belkin, 2009; Good et al., 2007; Signorini et al., 2015). The  
504 result of Seabra et al. (2019) in HuUS also showed a very similar trend ( $-0.07^{\circ}\text{C}$ ) compared with our OC1  
505 trend. Finally, in the BeUS, a good agreement is found with the average warming rate of Seabra et al.  
506 (2019). Our study demonstrates good agreement with existing literature on oceanic trends despite the

507 differences in methodologies employed. Our study demonstrates good agreement with existing literature  
508 on oceanic trends despite the differences in methodologies employed.

509 Although long-term changes, such as the North Atlantic Oscillation or the Pacific Oscillation, can impact  
510 the SST gradient, their effect would not surpass the ability of our analysis to support Bakun's hypothesis.  
511 In that sense, Nayaran et al. (2010) found that correlations between upwelling indices and climate indices  
512 like the Atlantic Multidecadal Oscillation Index (AMOI) lack significance. Similarly, the North Atlantic  
513 Oscillation Index (NAOI) exhibits a notable negative correlation with meridional wind stress off NW  
514 Africa, yet its correlation with the SST index remains insignificant. In the case of the CalUS, the Pacific  
515 Decadal Oscillation Index (PDOI) shows a weak but statistically significant correlation with the coastal  
516 upwelling SST index off California. However, no substantial correlation is found with alongshore wind  
517 stress. Cross-correlation analyses also reveal a lack of significant correlations across various time lags.  
518 On the other hand, (Bonino et al., 2019) found that local drivers and trends favoring upwelling (e.g.,  
519 equatorward wind stress, cyclonic wind stress curl, and thermocline depth variation) explain the low-  
520 frequency modulation of upwelling. Bonino et al. (2019) also explored the link between wind-based  
521 upwelling indices and climate modes. They found that Atlantic and Pacific upwelling variabilities are  
522 mainly independent, while intra-basin domain variabilities present some coherency, which is consistent  
523 with our results. This intra-basin covariability is especially marked in the Pacific Ocean, where the shared  
524 variability is majorly due to the El Niño Southern Oscillation (ENSO) mode. In contrast, in the Atlantic  
525 Ocean, coherent variability is associated with upwelling trends, whereas only in the CanUS is it linked to  
526 the AMO. These results suggest that long-term climate indices may influence coastal upwelling dynamics,  
527 which is especially important in the Pacific. However, our index,  $\alpha_{UI}$ , by normalizing the trend for its  
528 oceanic background, our results should account for the effects of local climate indices.

529 To assess Bakun's hypothesis and, thus, the upwelling capacity to overcome the oceanic warming effect,  
530 we define the angle ( $\alpha_{UI}$ , readers are referred to section 3.3) between oceanic water and upwelling trends.  
531 Because this new index is directly based on trends, it captures only the low-frequency variability.  
532 Additionally, we verified the method's robustness using a probabilistic assessment of the uncertainties  
533 that showed consistent intensifications for all EBUS (Fig 5). This new approach differs from the

534 traditional trend analysis since it normalizes the upwelling trends by comparing them with open ocean  
535 changes.

536 The EBUS in the Pacific Ocean yields minimum  $\alpha_{UI}$  ( $10^{\circ}\pm 3^{\circ}$  and  $14^{\circ}\pm 3^{\circ}$  for CalUS and HuUS,  
537 respectively), which is consistent with the low signal-to-noise ratio of global warming on this ocean,  
538 given its natural variability. The overall cooling signal caused by the IPO enhances the HuUS open ocean  
539 negative trends. Still, our index normalizes the upwelling trend to the full basin variability, suggesting the  
540 possibility of a mild Bakun effect even at the HuUS. In the Atlantic Ocean, the  $\alpha_{UI}$  for the CanUS and  
541 BeUS are  $20^{\circ}\pm 2^{\circ}$  and  $21^{\circ}\pm 2^{\circ}$ , respectively, twice as large as on the Pacific Ocean. The  $\alpha_{UI}$  presents wider  
542 angles at the southern hemisphere EBUS than in the northern hemisphere EBUS. Nevertheless, our results  
543 show a significant difference between oceanic and coastal trends reflected in positive  $\alpha_{UI}$  in all EBUS  
544 (Fig 5).

545 The SST changes in the EBUS respond mainly to changes in the upwelling processes which are ultimately  
546 driven by the pressure gradients. We analyzed the pressure gradients trends in all four EBUS. Our findings  
547 further support the intensification of the pressure gradients driven by climate change, as stated by Bakun  
548 (1990). However, there are probably other contributors to the intensification of the upwellings. Some  
549 researchers question whether the impacts of differential heating on the pressure gradient force drives  
550 intensification of coastal upwelling. Rather, a complementary hypothesis proposes that evidence of an  
551 intensifying pressure gradient force is limited to poleward migration of the Hadley Cell (Arellano and  
552 Rivas, 2019; Rykaczewski et al., 2015; Wang et al., 2015). Nevertheless, these projections are only  
553 supported by observational records in the Humboldt and Benguela Systems, (Sydeman et al., 2014). In  
554 contrast, we have tested this hypothesis on the historical record by computing the latitudinal distribution  
555 of  $\alpha_{UI}$ . The results shown in Fig 6 partially agree with Rykaczewski et al, (2015), as only CalUS and  
556 BeUS presented a poleward intensification of  $\alpha_{UI}$ . To further understand the drivers of these changes, we  
557 examined the spatial stability of the trends in the SLP continental-oceanic gradient was also tested using  
558 Monte Carlo simulation. The discrepancy between the latitudinal distribution of  $\alpha_{UI}$  and the small standard  
559 deviation of trends around the cores of the pressure systems suggests that the hypothesis of poleward  
560 displacement of the high-pressure systems remains inconclusive.



561 In summary, in this study, we use SST at discrete locations and the pressure gradient to explore the  
562 Bakun's hypothesis in the four major EBUS. Cooling trends are observed for all upwelling areas (the  
563 strongest in the HuUS and the weakest in the CalUS), and mainly warming trends offshore except for the  
564 HuUS. In addition, a novel index  $\alpha_{UI}$  that normalizes the upwelling trends to their background open ocean  
565 trend is proposed. This index is easy to estimate, allows interbasin trend comparisons, and helps  
566 understand the role of changing upwellings in a changing climate. The index reveals that the Bakun  
567 hypothesis remains a possible mechanism for upwelling intensification in all four EBUS, although the  
568 Atlantic Basin shows a higher intensification effect than the Pacific Ocean, and slightly stronger in the  
569 southern hemisphere than in the northern hemisphere.

#### 570 **Data availability.**

571 The moored data analyzed in this study are available  
572 at <https://www.ndbc.noaa.gov/> and <https://www.puertos.es/es-es/oceanografia/Paginas/portus.aspx> for  
573 the Pacific and Atlantic Ocean, respectively. The cruise data are also available  
574 at <https://calcofi.org/data/> for the Pacific Ocean and upon request from the author in the case of the  
575 Atlantic Ocean. And for the Satellite-based SST data, the NOAA reanalysis product  
576 are available from [https://www.ncei.noaa.gov/data/sea-surface-temperature-optimum-  
577 interpolation/access/avhrr-only/](https://www.ncei.noaa.gov/data/sea-surface-temperature-optimum-interpolation/access/avhrr-only/).

#### 578 **Author contribution**

579 M, Gutierrez-Guerra processed the data, and carried out all data analyses. M, Gutierrez-Guerra wrote the  
580 original paper with contributions from M, Gutierrez-Guerra, M.D, Perez-Hernandez and P, Velez. M.D,  
581 Perez-Hernandez and P, Velez supervised the study. All authors reviewed and edited the final paper.

#### 582 **Competing interests**

583 The contact author has declared that none of the authors has any competing interest.

584 **Acknowledges**

585 This article is a publication of the Unidad Océano y Clima from Universidad de Las Palmas de Gran  
586 Canaria, an R&D&I CSIC-associate unit. This work has been completed as part of the doctoral program  
587 in Oceanography and Global Change at the Instituto de Oceanografía y Cambio Global (IOCAG). M.A.  
588 Gutiérrez-Guerra acknowledges the Agencia Canaria de Investigación, Innovación y Sociedad de la  
589 Información (ACIISI) and the Fondo Social Europeo Plus (FSE+) Programa Operativo Integrado de  
590 Canarias 2021-2027, Eje 3 Tema Prioritario 74 (85%) grant program of “Apoyo al personal investigador en  
591 formación” FPI2024010234 and the INVESTIGO grant program of “Plan de Recuperación, Transformación  
592 y Resiliencia – Next Generation EU”.

593 **References**

- 594 Abbott, M. R. and Zion, P. M.: Spatial and temporal variability of phytoplankton pigment off northern  
595 California during Coastal Ocean Dynamics Experiment 1, *J Geophys Res Oceans*, 92, 1745–1755,  
596 <https://doi.org/10.1029/JC092IC02P01745>, 1987.
- 597 Abrahams, A., Schlegel, R. W., and Smit, A. J.: Variation and Change of Upwelling Dynamics Detected  
598 in the World’s Eastern Boundary Upwelling Systems, *Front Mar Sci*, 8, 626411,  
599 <https://doi.org/10.3389/FMARS.2021.626411/BIBTEX>, 2021.
- 600 Andrews, W. R. H. and Cram, D. L.: Combined Aerial and Shipboard Upwelling Study in the Benguela  
601 Current, *Nature* 1969 224:5222, 224, 902–904, <https://doi.org/10.1038/224902a0>, 1969.
- 602 Andrews, W. R. H. and Hutchings, L.: Upwelling in the Southern Benguela Current, *Prog Oceanogr*, 9,  
603 1–81, [https://doi.org/10.1016/0079-6611\(80\)90015-4](https://doi.org/10.1016/0079-6611(80)90015-4), 1980.
- 604 Arellano, B. and Rivas, D.: Coastal upwelling will intensify along the Baja California coast under  
605 climate change by mid-21st century: Insights from a GCM-nested physical-NPZD coupled numerical  
606 ocean model, *Journal of Marine Systems*, 199, 103207,  
607 <https://doi.org/10.1016/J.JMARSYS.2019.103207>, 2019.
- 608 Bakun, A.: Global climate change and intensification of coastal ocean upwelling, *Science* (1979), 247,  
609 198–201, <https://doi.org/10.1126/science.247.4939.198>, 1990.

610 Bakun, A. and Nelson, C. S.: The Seasonal Cycle of Wind-Stress Curl in Subtropical Eastern Boundary  
611 Current Regions, *J Phys Oceanogr*, 21, 1815–1834, [https://doi.org/https://doi.org/10.1175/1520-  
612 0485\(1991\)021<1815:TSCOWS>2.0.CO;2](https://doi.org/10.1175/1520-0485(1991)021<1815:TSCOWS>2.0.CO;2), 1991.

613 Bakun, A., Black, B. A., Bograd, S. J., García-Reyes, M., Miller, A. J., Rykaczewski, R. R., and  
614 Sydeman, W. J.: Anticipated Effects of Climate Change on Coastal Upwelling Ecosystems, *Curr Clim  
615 Change Rep*, 1, 85–93, <https://doi.org/10.1007/s40641-015-0008-4>, 2015.

616 Bang, N. and Andrews, W.: Direct current measurements of a shelf-edge frontal jet in the southern  
617 Benguela system, *J Mar Res*, 32, 1974.

618 Barton, E. D., Field, D. B., and Roy, C.: Canary current upwelling: More or less?, *Prog Oceanogr*, 116,  
619 167–178, <https://doi.org/10.1016/j.pocean.2013.07.007>, 2013.

620 Belkin, I. M.: Rapid warming of Large Marine Ecosystems, *Prog Oceanogr*, 81, 207–213,  
621 <https://doi.org/10.1016/j.pocean.2009.04.011>, 2009.

622 Benazzouz, A., Mordane, S., Orbi, A., Chagdali, M., Hilmi, K., Atillah, A., Lluís Pelegrí, J., and Hervé,  
623 D.: An improved coastal upwelling index from sea surface temperature using satellite-based approach –  
624 The case of the Canary Current upwelling system, *Cont Shelf Res*, 81, 38–54,  
625 <https://doi.org/10.1016/j.csr.2014.03.012>, 2014.

626 Bonino, G., Di Lorenzo, E., Masina, S., and Iovino, D.: Interannual to decadal variability within and  
627 across the major Eastern Boundary Upwelling Systems, *Scientific Reports* 2019 9:1, 9, 1–14,  
628 <https://doi.org/10.1038/s41598-019-56514-8>, 2019.

629 Cropper, T. E., Hanna, E., and Bigg, G. R.: Spatial and temporal seasonal trends in coastal upwelling  
630 off Northwest Africa, 1981–2012, *Deep Sea Research Part I: Oceanographic Research Papers*, 86, 94–  
631 111, <https://doi.org/10.1016/J.DSR.2014.01.007>, 2014.

632 Demarcq, H.: Trends in primary production, sea surface temperature and wind in upwelling systems  
633 (1998-2007), *Prog Oceanogr*, 83, 376–385, <https://doi.org/10.1016/j.pocean.2009.07.022>, 2009.

634 Dugdale, R. C. and Wilkerson, F. P.: New production in the upwelling center at Point Conception,  
635 California: temporal and spatial patterns, *Deep Sea Research Part A. Oceanographic Research Papers*,  
636 36, 985–1007, [https://doi.org/10.1016/0198-0149\(89\)90074-5](https://doi.org/10.1016/0198-0149(89)90074-5), 1989.

637 Ekman, V. W.: On the Influence of the Earth's Rotation on Ocean-Currents, Almqvist & Wiksells,  
638 Uppsala [Sweden], 1–52 pp., 1905.

639 Escribano, R., Daneri, G., Farías, L., Gallardo, V. A., González, H. E., Gutiérrez, D., Lange, C. B.,  
640 Morales, C. E., Pizarro, O., Ulloa, O., and Braun, M.: Biological and chemical consequences of the  
641 1997–1998 El Niño in the Chilean coastal upwelling system: a synthesis, *Deep Sea Research Part II:*  
642 *Topical Studies in Oceanography*, 51, 2389–2411, <https://doi.org/10.1016/J.DSR2.2004.08.011>, 2004.

643 Figueroa, D. and Moffat, C.: On the influence of topography in the induction of coastal upwelling along  
644 the Chilean Coast, *Geophys Res Lett*, 27, 3905–3908, <https://doi.org/10.1029/1999GL011302>, 2000.

645 García-Reyes, M., Sydeman, W. J., Schoeman, D. S., Rykaczewski, R. R., Black, B. A., Smit, A. J., and  
646 Bograd, S. J.: Under pressure: Climate change, upwelling, and eastern boundary upwelling ecosystems,  
647 *Front Mar Sci*, 2, 1–10, <https://doi.org/10.3389/fmars.2015.00109>, 2015.

648 Gómez-Gesteira, M., De Castro, M., Álvarez, I., Lorenzo, M. N., Gesteira, J. L. G., and Crespo, A. J.  
649 C.: Spatio-temporal upwelling trends along the Canary upwelling system (1967-2006), *Ann N Y Acad*  
650 *Sci*, 1146, 320–337, <https://doi.org/10.1196/annals.1446.004>, 2008.

651 Good, S. A., Corlett, G. K., Remedios, J. J., Noyes, E. J., and Llewellyn-Jones, D. T.: The global trend  
652 in sea surface temperature from 20 years of advanced very high resolution radiometer data, *J Clim*, 20,  
653 1255–1264, <https://doi.org/10.1175/JCLI4049.1>, 2007.

654 Good, S. A., Martin, M. J., and Rayner, N. A.: EN4: Quality controlled ocean temperature and salinity  
655 profiles and monthly objective analyses with uncertainty estimates, *J Geophys Res Oceans*, 118, 6704–  
656 6716, <https://doi.org/10.1002/2013JC009067>, 2013.

657 Hutchings, L., van der Lingen, C. D., Shannon, L. J., Crawford, R. J. M., Verheye, H. M. S.,  
658 Bartholomae, C. H., van der Plas, A. K., Louw, D., Kreiner, A., Ostrowski, M., Fidel, Q., Barlow, R.  
659 G., Lamont, T., Coetzee, J., Shillington, F., Veitch, J., Currie, J. C., and Monteiro, P. M. S.: The  
660 Benguela Current: An ecosystem of four components, *Prog Oceanogr*, 83, 15–32,  
661 <https://doi.org/10.1016/j.pocean.2009.07.046>, 2009.

662 Kämpf, J. and Chapman, P.: *Upwelling Systems of the World*, [https://doi.org/10.1007/978-3-319-](https://doi.org/10.1007/978-3-319-42524-5)  
663 42524-5, 2016.

664 Kang, S. M., Yu, Y., Deser, C., Zhang, X., Kang, I. S., Lee, S. S., Rodgers, K. B., and Ceppi, P.: Global  
665 impacts of recent Southern Ocean cooling, *Proc Natl Acad Sci U S A*, 120, e2300881120,  
666 [https://doi.org/10.1073/PNAS.2300881120/SUPPL\\_FILE/PNAS.2300881120.SAPP.PDF](https://doi.org/10.1073/PNAS.2300881120/SUPPL_FILE/PNAS.2300881120.SAPP.PDF), 2023a.

667 Kang, S. M., Ceppi, P., Yu, Y., and Kang, I. S.: Recent global climate feedback controlled by Southern  
668 Ocean cooling, *Nature Geoscience* 2023 16:9, 16, 775–780, [https://doi.org/10.1038/s41561-023-01256-](https://doi.org/10.1038/s41561-023-01256-6)  
669 6, 2023b.

670 Kendall, M.: Rank correlation methods (4th edn.) Charles Griffin, San Francisco, CA, 8, 875, 1975.

671 Lutjeharms, J. R. E. and Meeuwis, J. M.: The extent and variability of South-East Atlantic upwelling,  
672 *South African Journal of Marine Science*, 5, 51–62, <https://doi.org/10.2989/025776187784522621>,  
673 1987.

674 Mann, H. B.: Nonparametric Tests Against Trend, *Econometrica*, 13, 245,  
675 <https://doi.org/10.2307/1907187>, 1945.

676 Marín, C.: Upwelling shadows at Mejillones Bay (northern Chilean coast): a remote sensing in situ  
677 analysis, *Investigaciones Marinas*, 31, 47–55, 2003.

678 McGregor, H. V., Dima, M., Fischer, H. W., and Mulitza, S.: Rapid 20th-century increase in coastal  
679 upwelling off northwest Africa, *Science* (1979), 315, 637–639,  
680 <https://doi.org/10.1126/science.1134839>, 2007.

681 Meehl, G. A., Hu, A., Santer, B. D., and Xie, S. P.: Contribution of the Interdecadal Pacific Oscillation  
682 to twentieth-century global surface temperature trends, *Nature Climate Change* 2016 6:11, 6, 1005–  
683 1008, <https://doi.org/10.1038/nclimate3107>, 2016.

684 Mesias, J. M., Matano, R. P., and Strub, P. T.: Dynamical analysis of the upwelling circulation off  
685 central Chile, *J Geophys Res Oceans*, 108, 3085, <https://doi.org/10.1029/2001JC001135>, 2003.

686 Narayan, N., Paul, A., Mulitza, S., and Schulz, M.: Trends in coastal upwelling intensity during the late  
687 20th century, *Ocean Science*, 6, 815–823, <https://doi.org/10.5194/OS-6-815-2010>, 2010.

688 Pauly, D. and Christensen, V.: Primary production required to sustain global fisheries, *Nature*, 376,  
689 279–279, <https://doi.org/10.1038/376279b0>, 1995.

690 Peard, K. R.: Seasonal and interannual variability of wind-driven upwelling at Lüderitz, Namibia,  
691 <http://hdl.handle.net/11427/6498>, 2007.

692 Reynolds, R. W., Smith, T. M., Liu, C., Chelton, D. B., Casey, K. S., and Schlax, M. G.: Daily high-  
693 resolution-blended analyses for sea surface temperature, *J Clim*, 20, 5473–5496,  
694 <https://doi.org/10.1175/2007JCLI1824.1>, 2007.

695 Rykaczewski, R. R., Dunne, J. P., Sydemann, W. J., García-Reyes, M., Black, B. A., and Bograd, S. J.:  
696 Poleward displacement of coastal upwelling-favorable winds in the ocean’s eastern boundary currents  
697 through the 21st century, *Geophys Res Lett*, 42, 6424–6431, <https://doi.org/10.1002/2015GL064694>,  
698 2015.

699 Sambe, B., Tandstad, M., Caramelo, A. M., and Brown, B. E.: Variations in productivity of the Canary  
700 Current Large Marine Ecosystem and their effects on small pelagic fish stocks, *Environ Dev*, 17, 105–  
701 117, <https://doi.org/10.1016/j.envdev.2015.11.012>, 2016.

702 Santos, F., deCastro, M., Gómez-Gesteira, M., and Álvarez, I.: Differences in coastal and oceanic SST  
703 warming rates along the Canary upwelling ecosystem from 1982 to 2010, *Cont Shelf Res*, 47, 1–6,  
704 <https://doi.org/10.1016/j.csr.2012.07.023>, 2012.

705 Seabra, R., Varela, R., Santos, A. M., Gómez-Gesteira, M., Meneghesso, C., Wetthey, D. S., and Lima,  
706 F. P.: Reduced nearshore warming associated with eastern boundary upwelling systems, *Front Mar Sci*,  
707 6, 445128, <https://doi.org/10.3389/FMARS.2019.00104/BIBTEX>, 2019.

708 Sherman, K. and Hempel, G.: The UNEP Large Marine Ecosystem Report: A perspective on changing  
709 conditions in LMEs of the world’s Regional Seas, *UNEP Regional Seas Reports and Studies*, 2008.

710 Siemer, J. P., Machín, F., González-Vega, A., Arrieta, J. M., Gutiérrez-Guerra, M. A., Pérez-  
711 Hernández, M. D., Vélez-Belchí, P., Hernández-Guerra, A., and Fraile-Nuez, E.: Recent Trends in SST,  
712 Chl-a, Productivity and Wind Stress in Upwelling and Open Ocean Areas in the Upper Eastern North  
713 Atlantic Subtropical Gyre, *J Geophys Res Oceans*, 126, e2021JC017268,  
714 <https://doi.org/10.1029/2021JC017268>, 2021.

715 Signorini, S. R., Franz, B. A., and McClain, C. R.: Chlorophyll variability in the oligotrophic gyres:  
716 Mechanisms, seasonality and trends, *Front Mar Sci*, 2, 1–11, <https://doi.org/10.3389/fmars.2015.00001>,  
717 2015.

718 Smale, D. A. and Wernberg, T.: Satellite-derived SST data as a proxy for water temperature in  
719 nearshore benthic ecology, *Mar Ecol Prog Ser*, 387, 27–37, <https://doi.org/10.3354/MEPS08132>, 2009.

720 Sydeman, W. J., García-Reyes, M., Schoeman, D. S., Rykaczewski, R. R., Thompson, S. A., Black, B.  
721 A., and Bograd, S. J.: Climate change and wind intensification in coastal upwelling ecosystems, *Science*  
722 (1979), 345, 77–80, <https://doi.org/10.1126/science.1251635>, 2014.

723 Tel, E., Balbin, R., Cabanas, J. M., Garcia, M. J., Carmen Garcia-Martinez, M., Gonzalez-Pola, C.,  
724 Lavin, A., Lopez-Jurado, J. L., Rodriguez, C., Ruiz-Villarreal, M., Sánchez-Leal, R. F., Vargas-Yáñez,  
725 M., and Vélez-Belchí, P.: IEOOS: The Spanish Institute of Oceanography Observing System, *Ocean*  
726 *Science*, 12, 345–353, <https://doi.org/10.5194/OS-12-345-2016>, 2016.

727 Wang, D., Gouhier, T. C., Menge, B. A., and Ganguly, A. R.: Intensification and spatial  
728 homogenization of coastal upwelling under climate change, *Nature*, 518, 390–394,  
729 <https://doi.org/10.1038/nature14235>, 2015.

730